Mapping eQTL networks with mixed graphical models

Inma Tur[1,2], Alberto Roberato[3], Robert Castelo[1,2,*]

1 Dept. Experimental and Health Sciences, Universitat Pompeu Fabra, Barcelona, Spain.

2 Research Program on Biomedical Informatics, Institut de Recerca Hospital del Mar, Barcelona, Spain.

3 Department of Statistical Sciences, Università di Bologna, Italy.

* Corresponding author: robert.castelo@upf.edu

arXiv:1402.4547v2 [q-bio.QM] 20 Feb 2014

Abstract

Expression quantitative trait loci (eQTL) mapping constitutes a challenging problem due to, among other reasons, the high-dimensional multivariate nature of gene expression traits. Next to the expression heterogeneity produced by confounding factors and other sources of unwanted variation, indirect effects spread throughout genes as a result of genetic, molecular and environmental perturbations. Disentangling direct from indirect effects while adjusting for unwanted variability should help us moving from current parts list of molecular components to understanding how these components work together. In this paper we approach this challenge with mixed graphical Markov models and higher-order conditional independences. To unlock this methodological framework we derive the parameters for an exact likelihood ratio test and demonstrate its fundamental relevance for higher-order conditioning on continuous expression and discrete genotypes. These models show that additive genetic effects propagate through the network as function of gene-gene correlations. The estimation of the eQTL network underlying a well-studied yeast data set using our methodology leads to a sparse structure with more direct genetic and regulatory associations that enable a straightforward comparison of the genetic control of gene expression across chromosomes. More importantly, it reveals that the larger genetic effects are *trans*-acting on genes located in a different chromosome and with a high number of connections to other genes in the network.

Introduction

The simultaneous assay of gene expression profiling and genotyping on the same samples with high-throughput technologies provides one of the primary types of integrative genomics data sets, the so-called *genetical genomics* data [26]. First studies producing such data showed that, for many genes, gene expression is an heritable trait [7]. Following this observation, it soon became evident that gene expression may act as an intermediate data tier which can potentially increase our power to map the genetic component of phenotypic variability in complex traits such as human disease [53]. The genetic variants associated to each of these thousands of molecular phenotypes are known as expression quantitative trait loci (eQTL) and they can be broadly categorized into *cis*-acting and *trans*-acting associations, depending on their location relative to the gene whose expression levels map to the eQTL[1]. Because the relative concentration of RNA molecules reflects functional relationships between genes, overlaying the correlation structure of gene expression on the

[1]We use here the terms *cis* and *trans* to refer to what is also known as *local* and *distant* QTLs [51], respectively.

eQTL associations provides an *eQTL network* which can help to approach the problem of reverse engineering the genotype-phenotype map with natural variation [50].

A straightforward way to map eQTL networks to the genome is by treating gene expression profiles as independent continuous traits and applying classical QTL mapping techniques such as single marker regression [58]. However, differently to higher-level phenotypes such as disease onset, adult height or yeast growth rates, gene expression is a high-dimensional multivariate trait involving measurements from thousands of genes coordinately acting under complex molecular regulatory programs. This feature makes eQTL mapping a challenging problem for, at least, two reasons. One is that gene expression profiles can be highly correlated as product of gene regulation, thereby complicating the distinction between direct and indirect effects when marginally inspecting eQTL associations that only involve one gene at a time. The other is that high-throughput expression profiling can be very sensitive to non-biological factors of variation such as batch effects [37, 36], introducing heterogeneity and spurious correlations between gene expression measurements. These artifacts may compromise the statistical power to map truly biological eQTLs [57] or show up as interesting genetic switches with broad pleiotropic effects affecting a large number of genes, commonly known as eQTL hotspots [37, 5].

These problems can be addressed by estimating and including the confounding factors in the model as main [37, 57] or mixed effects [29, 40] and restricting the eQTL search to *cis*-acting variants located in the regulatory regions of the gene to which they are associated [43].

Yet, *trans*-acting eQTL have proven to be crucial to our understanding of complex regulatory mechanisms. A canonical example are locus control regions [39] that enhance the expression of distal genes under tissue specific conditions such as the one affecting the human β-globin locus [23]. More recent contributions have shown that *trans*-acting mechanisms often mediate the genetic basis of disease [21, 59].

The importance of identifying non-spurious *trans*-acting eQTL has been widely recognized and a large number of approaches exist in the literature that aim to address the problems described above. They can be broadly categorized into those extending univariate single marker regression models to adjust for confounding effects [37, 57, 40] and those using multivariate approaches. The latter can be further categorized into Bayesian networks using conditional mutual information with constraint-based algorithms [61], empirical Bayes hierarchical mixtures [30], structural equation models [41], sparse partial least squares [15], fused lasso regression methods [31], random forests [42], Bayesian networks using the BIC criterion with score-based algorithms [45], mixed graphical models restricted to tree network topologies [20], sparse factor analysis [47], and conditional independence tests of order one [3, 12, 44, 28].

All these approaches integrate a gene regulatory network model into the QTL mapping framework to provide a systems view of the underlying genotype-phenotype map. While every of these models approach in some way the challenge of distinguishing direct from indirect eQTL and gene-gene associations, their interpretation becomes harder with the increasing complexity of the underlying statistical principles in which many of them are based.

On the other hand, mixed graphical models and conditional independence constitute a natural extension of classical QTL mapping to multivariate phenotype vectors. This enables a smooth transition from mapping single phenotypes to building eQTL networks providing an easier statistical interpretation of the resulting associations.

However, currently available methods based on mixed graphical models and conditional independence [20, 3, 12, 44, 28] present two main shortcomings. Firstly, they are restricted to conditioning on one other gene to disentangle direct and indirect relationships. Secondly, their underlying statistical principles governing the flow of additive and linear effects going from genetic variants to continuous phenotypes throughout gene expression are poorly understood in the genetics community.

The main purpose of this paper is to unlock the application of higher-order conditional independence and mixed graphical models to eQTL mapping. More concretely, we show (i) how additive effects from genetic variants propagate to gene expression and continuous phenotypes as function of linear effects among the genes; (ii) how to test for conditional independence between a discrete genetic variant and a Gaussian distributed phenotype *exactly*, as opposed to using the classical χ^2 *asymptotic* test, and why this is important when testing higher-order associations; (iii) how can we use conditional independence to adjust for the expression of every other gene, other covariates and confounding factors in genetical genomics data; (iv) what kind of statistical model one may expect to find as function of the order of the conditional associations; (v) how this framework provides a seamless connection from genetic variants to gene networks, while facilitating the interpretation in terms of conditional independences; and (vi) how the resulting sparser eQTL networks fit better the data and provide valuable insight into the genetic regulatory architecture of gene expression in yeast.

Materials and Methods

Expression measurements and genotyping

Throughout this paper we use a well-studied real genetical genomics data set [6] from a study where two yeast strains, a wild-type (RM11-1a) and a lab strain (BY4716), were

crossed to generate 112 segregants which were genotyped and whose gene expression was profiled using two-channel microarray chips, including a dye-swap [6].

We applied background correction, discarded control probes and normalized the raw expression data within and between arrays using the `limma` package [55]. To correct for possible dye effects, we averaged the normalized expression values of the dye-swapped arrays. This first set of normalized data consisted of 6,216 genes and 2,906 genotype markers, i.e., a total of $p = 9,122$ features, by $n = 112$ samples.

We observed that there were sets of genotype markers clustered in genomic regions with identical genotypes. We sought the genes with highest LOD scores to each of these clusters of markers. When the gene was located in a different chromosome a marker was arbitrarily selected within its cluster. When the gene was located in the same chromosome, the closest marker to the gene was selected. The rest of identical markers were discarded from further analysis. We also removed genes whose annotation did not map to the April 2011 version of the yeast genome (sacCer3) at the UCSC Genome Browser (`http://www.genome.ucsc.edu`). This resulted in a final data set of 2,150 markers and 6,104 genes, i.e., a total of $p = 8,254$ features, by $n = 112$ samples.

Mixed Graphical Markov models of eQTL networks

Disentangling direct and indirect associations of genes and genetic variants through gene expression and natural variation requires some underlying model of the eQTL network. We assumed that gene expression forms a p-multivariate sample following a conditional Gaussian distribution given the joint probability of all genetic variants. Under this assumption a sensible model for an eQTL network is a mixed graphical Markov model -GMM- [34]. A mixed GMM enables the integration of the joint distribution of discrete genotypes with the joint distribution of continuous expression measurements in a single multivariate statistical model satisfying a set of restrictions of conditional independence encoded by means of a graph; see [33, 19] for a comprehensive description of this type of statistical model.

Here, we review part of the mixed GMM theory required for this paper. Mixed GMMs are statistical models representing probability distributions involving discrete random variables (r.v.'s), denoted by I_δ with $\delta \in \Delta$, and continuous r.v.'s, denoted by Y_γ with $\gamma \in \Gamma$. This class of GMMs are determined by undirected marked graphs $G = (V, E)$ with p marked vertices $V = \Delta \cup \Gamma$, and edge set $E \subseteq V \times V$. Vertices $\delta \in \Delta$ are depicted by solid circles, $\gamma \in \Gamma$ by open ones and the entire set of them, V, index the vector of r.v.'s $X = (I, Y)$. In our context, continuous r.v.'s Y correspond to genes and discrete r.v.'s I to markers or eQTLs; see Figure 1a for a graphical representation of one such

mixed GMM. We denote the joint sample space of X by:

$$x = (i, y) = \{(i_\delta)_{\delta\in\Delta}, (y_\gamma)_{\gamma\in\Gamma}\} \,, \tag{1}$$

where i_δ are discrete values corresponding to genotype alleles from the marker or eQTL I_δ and y_γ are continuous values of expression from gene Y_γ. The set of all possible joint discrete levels i is denoted as $\mathcal{I}$. Following [34], we assume that the joint distribution of the variables X is conditional Gaussian (also known as CG-distribution) with density function:

$$f(x) = f(i, y) = p(i)|2\pi\Sigma(i)|^{-\frac{1}{2}} \times \exp\left\{-\frac{1}{2}(y - \mu(i))^T\Sigma(i)^{-1}(y - \mu(i))\right\} . \tag{2}$$

This distribution has the property that continuous variables follow a multivariate normal distribution $\mathcal{N}_{|\Gamma|}(\mu(i), \Sigma(i))$ conditioned on the discrete variables. The parameters $(p(i), \mu(i), \Sigma(i))$ are called moment characteristics where $p(i)$ is the probability that $I = i$, and $\mu(i)$ and $\Sigma(i)$ are the conditional mean and the covariance matrix of Y which depends on i. If the covariance matrix is constant across the levels of $\mathcal{I}$, that is, $\Sigma(i) \equiv \Sigma$, the model is *homogeneous*. Otherwise, the model is said to be *heterogeneous*.

We can write the logarithm of the density in terms of the canonical parameters $(g(i), h(i), K(i))$:

$$\log f(i, y) = g(i) + h(i)^T y - \frac{1}{2}y^T K(i) y \,, \tag{3}$$

where

$$\begin{aligned} g(i) &= \log(p(i)) - \frac{1}{2}\log|\Sigma(i)| - \frac{1}{2}\mu(i)^T\Sigma(i)^{-1}\mu(i) - \frac{|\Gamma|}{2}\log(2\pi) \,, & (4)\\ h(i) &= \Sigma(i)^{-1}\mu(i) \,, & (5)\\ K(i) &= \Sigma(i)^{-1} \,. & (6) \end{aligned}$$

CG-distributions satisfy the Markov property if and only if their canonical parameters are expanded into interaction terms such that only those interactions among adjacent vertices are present [33]. Thus,

$$g(i) = \sum_{d\subseteq\Delta} \lambda_d(i) \,, \quad h_\gamma(i) = \sum_{d\subseteq\Delta} \eta_d(i)_\gamma, \quad k_{\gamma\eta}(i) = \sum_{d\subseteq\Delta} \psi_d(i)_{\gamma\eta} \,, \tag{7}$$

where $\lambda_d(i)$, with $d \subseteq \Delta$ complete in G, represent the discrete interactions among the variables indexed by d; $\eta_d(i)_\gamma$, with $d\cup\{\gamma\}$ complete in G, represent the mixed interactions between X_γ and the variables indexed by d; and $\psi_d(i)_{\gamma\eta}$, with $d \cup \{\gamma, \eta\}$ complete in G, represent the quadratic interactions between X_γ, X_η and the variables indexed by d. If

the model is homogeneous, there are not mixed quadratic interactions, i.e., $\psi_d(i)_{\gamma\eta} = 0$ for $d \neq \emptyset$. Plugging these expansions in Eq. (3) we obtain

$$\log f(i,y) = \sum_{d\subseteq\Delta} \lambda_d(i) + \sum_{d\subseteq\Delta}\sum_{\gamma\in\Gamma} \eta_d(i)_\gamma y_\gamma - \frac{1}{2}\sum_{d\subseteq\Delta}\sum_{\gamma,\eta\in\Gamma} \psi_d(i)_{\gamma\eta} y_\gamma y_\eta \,, \tag{8}$$

where $\lambda_d(i) = 0$ unless d is complete in G, $\eta_d(i)_\gamma = 0$ unless $d \cup \{\gamma\}$ is complete in G, and $\psi_d(i)_{\gamma\eta} = 0$ unless $d \cup \{\gamma,\eta\}$ is complete in G.

Decomposable mixed GMMs

An important subclass of mixed GMMs is defined by decomposable marked graphs.

Definition 1. A triple (A, B, C) of disjoint subsets of V form a decomposition of an undirected marked graph G if $V = A \cup B \cup C$ and: (1) C is a complete subset of V; (2) C separates A from B; and (3) $C \subseteq \Delta$ or $B \subseteq \Gamma$.

An undirected marked graph G is said to be *decomposable* if it is complete, or if there exists a proper decomposition (A, B, C) such that the subgraphs $G_{A\cup C}$ and $G_{B\cup C}$ are decomposable. In different terms, when G is undirected, decomposability of G holds if and only if G does not contain chordless cycles of length larger than 3 and does not contain any path between two non-adjacent discrete vertices passing through continuous vertices only.

Maximum Likelihood Estimates of mixed GMMs

Let $\mathcal{X} = \{x^{(\nu)}\} = \{(i^{(\nu)}, y^{(\nu)})\}$ be a sample of $\nu = 1, ..., n$ independent and identically distributed observations from a CG-distribution. For an arbitrary subset $A \subseteq V$, we abbreviate to $i_A = i_{A\cap\Delta}$, $\mathcal{I}_A = \mathcal{I}_{\Delta\cap A}$ and $y_A = y_{A\cap\Gamma}$ and the following sampling statistics are defined:

$$\begin{aligned}
n(i) &= \#\{\nu : i^{(\nu)} = i\} && (9)\\
s(i) &= \sum_{\nu: i^{(\nu)}=i} y^{(\nu)} && (10)\\
\bar{y}(i) &= s(i)/n(i) && (11)\\
ss(i) &= \sum_{\nu: i^{(\nu)}=i} y^{(\nu)}(y^{(\nu)})^T && (12)\\
ssd(i) &= ss(i) - s(i)s(i)^T/n(i) && (13)\\
ssd_A(A) &= \sum_{i_A\in\mathcal{I}_A} ssd_{A\cap\Gamma}(i_A) && (14)
\end{aligned}$$

The likelihood function for the homogeneous, saturated model attains its maximum if

and only if $n \geq |\Gamma| + |\mathcal{I}|$, which is almost surely to $n(i) > 0$ for all $i \in \mathcal{I}$ [33], Prop. 6.10. In such a case, the MLEs of the moment characteristics are defined as follows:

$$\hat{p}(i) = n(i)/n, \quad \hat{\mu}(i) = \bar{y}(i), \quad \hat{\Sigma} = ssd_V(V)/n = ssd/n\,. \tag{15}$$

However, in this case, it follows that saturated mixed GMMs cannot be directly estimated from data with $p \gg n$, using only the formulas described above.

For the unsaturated case, decomposable mixed GMMs also admit explicit MLEs. In the homogeneous case it can be shown [33, Prop. 6.21] that the MLE exists almost surely if and only if $n(i_C) \geq |C \cap \Gamma| + |\mathcal{I}_C|$ for all cliques C of G and $i_C \in \mathcal{I}_C$. In this case, MLEs are defined with the following canonical parameters [33, pg. 189]:

$$\hat{p}(i) = \prod_{j=1}^{k} \frac{n(i_{C_j})}{n(i_{S_j})}\,, \tag{16}$$

$$\hat{h}(i) = n\left\{ \sum_{j=1}^{k} \left[ssd_{C_j}(C_j)^{-1}\bar{y}_{C_j}(i_{C_j})\right]^{|\Gamma|} - \left[ssd_{S_j}(S_j)^{-1}\bar{y}_{S_j}(i_{S_j})\right]^{|\Gamma|} \right\}, \tag{17}$$

$$\hat{K} = n\left\{ \sum_{j=1}^{k} \left[ssd_{C_j}(C_j)^{-1}\right]^{|\Gamma|} - \left[ssd_{S_j}(S_j)^{-1}\right]^{|\Gamma|} \right\}, \tag{18}$$

where $S_1 = \emptyset$.

The matrices $[M]^{|\Gamma|}$ of Equation (18) are defined as follows. Given a matrix $M = \{m_{\gamma\eta}\}_{|A|\times|A|}$ of dimension $|A| \times |A|$ with $A \subseteq \Gamma$, $[M]^{|\Gamma|}$ is a $|\Gamma| \times |\Gamma|$ matrix such that,

$$[M]^{|\Gamma|}_{\gamma\eta} = \begin{cases} m_{\gamma\eta}, & \text{if } \{\gamma, \eta\} \in A\,, \\ 0, & \text{otherwise}\,. \end{cases}$$

Analogously, in Equation (17), $[M]^{|\Gamma|}$ is a $|\Gamma|$-length vector obtained from a $|A|$-length vector M.

Simulation of eQTL network models with mixed GMMs

In this subsection, we describe how to simulate eQTL networks with homogeneous mixed GMMs and data from them. Here, we restrict ourselves to the case of a backcross, in which each genotype marker can have two different genotypic values, but the simulations could be extended to other cross models allowing for other than linear additive effects (codominant model) on the mixed associations, such as dominance effects. As shown in the Results section, such an exercise enables gathering a deeper understanding into the flow of genetic additive effects arising from eQTL and propagating through the gene

network under this type of models.

Simulation of eQTL network structures

The first step to simulate a GMM consists of simulating its associated graph $G = (V, E)$ which, in this case, defines the structure of the eQTL network. Discrete r.v's. I, associated to discrete vertices Δ correspond to eQTLs and continuous r.v.'s Y associated to continuous vertices Γ to expression profiles, such that $V = \Delta \cup \Gamma$ and $|V| = p$. In the context of genetical genomics data we make the assumption that discrete genotypes affect gene expression measurements and not the other way around. Thus, we consider the underlying graph G as a marked graph with mixed edges, where some are directed and represented by arrows and some are undirected. More concretely, G will have arrows pointing from discrete vertices to continuous ones, undirected edges between continuous vertices and no edges between discrete vertices. From this restriction, it follows immediately that there are no semi-directed cycles and allows one to interpret these GMMs as *chain graphs*, which are graphs formed by undirected subgraphs connected by directed edges [33].

One of the basic assumptions made by procedures that estimate the structure of GMMs when $p \gg n$ is that the underlying graph structure is sparse. In the present context, this means that the number of eQTLs and gene-gene associations present in the eQTL network is much smaller than their total possible number. Therefore, to explore the performance of estimation procedures, we are interested in sampling graphs with a fine-tune control of the level of sparseness. In our case, we sample the undirected subgraph that defines the gene network from the subclass of undirected d-regular graphs [24, 56]. These are graphs with a constant vertex degree d which makes the graph density D a linear function of d, $D = d/(p_\Gamma - 1)$, where $p_\Gamma = |\Gamma|$ is the number of genes and $p_\Gamma \cdot d$ is even because otherwise it not d-regular [24]. The constant degree d also bounds the size of any minimal subset separating every pair of vertices [10, pg. 2646]. Finally, we restrict eQTL relationships, which correspond to directed mixed edges, to at most one per gene.

Simulation of parameters of a homogeneous mixed GMM

After simulating the underlying graph structure G, we need to simulate the parameters of the CG-distribution represented by G with given marginal linear correlations of magnitude ρ on the pure continuous (gene-gene) associations and given additive effects of magnitude a on the mixed eQTL ones. We simulate *homogeneous* mixed GMMs. In the context of genetical genomics data, this assumption implies that genotype affects only the mean expression level of genes and not the correlations between them.

Conditional covariance matrix: Once the structure of the graph G is obtained,

a random homogeneous conditional covariance matrix Σ is generated as follows. Let $G_\Gamma \subseteq G$ denote the subgraph of $p_\Gamma = |\Gamma|$ pure continuous vertices and let ρ denote the desired mean marginal correlation between each pair of continuous r.v.'s (X_γ, X_η) such that $(\gamma, \eta) \in G_\Gamma$. Let $\mathcal{S}^+(G_\Gamma) \subset \mathcal{S}^+$ denote the set of all $p_\Gamma \times p_\Gamma$ positive definite matrices in $\mathcal{S}^+$ such that every matrix $S \in \mathcal{S}^+(G_\Gamma)$ satisfies that $\{S^{-1}\}_{ij} = 0$ whenever $i \neq j$ and $(i, j) \notin G_\Gamma$.

We simulate Σ such that $\Sigma \in \mathcal{S}^+(G_\Gamma)$ in two steps. First, we build an initial positive definite matrix $\tilde{\Sigma}_0 \in \mathcal{S}^+$ and from this, we build the *incomplete matrix* Σ_0 with elements $\{\sigma^0_{ij}\}$ if either $i = j$ or $(i, j) \in G_\Gamma$, and the remaining elements unspecified. Second, we search for a *positive completion* of Σ_0, which consists of filling up Σ_0 in such a way that the resulting $\Sigma \in \mathcal{S}^+(G_\Gamma)$.

It can be shown [22] that the incomplete matrix Σ_0 admits a positive completion and that it is unique. This means that, given Σ_0, we can use algorithms for maximum likelihood estimation or Bayesian conjugate inference [52] as matrix completion algorithms. To this end, we first draw Σ_0 from a Wishart distribution $W_{p_\Gamma}(\Lambda, p_\Gamma)$ with $\Lambda = D\tilde{\Sigma}_0 D, D = \text{diag}(\{\sqrt{1/p_\Gamma}\}_{p_\Gamma})$ and $\tilde{\Sigma}_0 = \{\tilde{\Sigma}_{0_{ij}}\}_{p_\Gamma \times p_\Gamma}$ where $\tilde{\Sigma}_{0_{ij}} = 1$ for $i = j$ and $\tilde{\Sigma}_{0_{ij}} = \rho$ for $i \neq j$. It is required that $\Lambda \in \mathcal{S}^+$ and this happens if and only if $-1/(p_\Gamma - 1) < \rho < 1$ [54, pg. 317]. Finally, we apply the iterative regression procedure introduced by [25, pg. 634] for maximum likelihood estimation of Gaussian graphical models as matrix completion algorithm to obtain Σ from Σ_0.

Probability of discrete levels: since we are simulating a backcross, each discrete r.v. takes two possible values $i_\delta = \{1, 2\}$ with equal probability $p(i_\delta = 1) = p(i_\delta = 2) = 0.5$. For the purpose of simulating eQTL networks we made the simplifying assumption that discrete r.v.'s representing eQTLs are marginally independent between them. From these two assumptions it follows that joint levels $i \in \mathcal{I}$ are uniformly distributed, that is, $p(i) = 1/|\mathcal{I}| \ \forall i \in \mathcal{I}$.

Conditional mean vector: the values of the mean vector $\mu(i)$ are determined from the strength of the mixed interactions between discrete and continuous r.v.'s. Thus, we force each discrete variable I_δ to have an additive effect $a_{\delta\gamma}$ on the continuous variable Y_γ which, for the case of a backcross, implies that:

$$a_{\delta\gamma} = \mu_\gamma(1) - \mu_\gamma(2) = \frac{1}{|\mathcal{I}|/2} \sum_{i':i_\delta=1} \mu(i') - \frac{1}{|\mathcal{I}|/2} \sum_{i':i_\delta=2} \mu(i')\,, \tag{19}$$

where the random vector $\mu(i)$, conditioned on the discrete levels $\mathcal{I}$, is generated from (5). The values of the canonical parameter $h(i) = \{h_\gamma(i)\}_{\gamma\in\Gamma}$, determine the strength of the mixed interactions between discrete and continuous r.v.'s. and they are generated as in

(7). In particular,

$$h_\gamma(i) = \begin{cases} \eta_{\emptyset\gamma}, & \text{if } (\delta,\gamma) \notin E \ \forall \delta \in \Delta. \\ \{\eta_\delta(i_\delta)_\gamma\}_{i_\delta \in \mathcal{I}_\delta} = \{\eta_\delta(1)_\gamma, \eta_\delta(2)_\gamma\}, & \text{if } (\delta,\gamma) \in E,\ \delta \in \Delta. \end{cases}$$

Without loss of generality, the values $\eta_{\emptyset\gamma}$ are set to zero. To set the values $\eta_\delta(1)_\gamma$ and $\eta_\delta(2)_\gamma$ so that both (5) and (19) are satisfied we proceed as follows. Assume that a genotype represented by a r.v. I_δ has a pleiotropic effect on a set of genes corresponding to r.v.'s $\{Y_\gamma\}_{\gamma \in A_\delta}$, where $A_\delta = \{\gamma \in \Gamma : (\delta,\gamma) \in E\}$. By combining (5) and (19), for each $\gamma \in A_\delta$, we have that

$$\begin{aligned} a_{\delta\gamma} &= \frac{1}{|\mathcal{I}|/2} \sum_{i':i_\delta=1} \sum_{\zeta\in\Gamma} \sigma_{\gamma\zeta} h_\zeta(i') - \frac{1}{|\mathcal{I}|/2} \sum_{i':i_\delta=2} \sum_{\zeta\in\Gamma} \sigma_{\gamma\zeta} h_\zeta(i') = \\ &= \frac{1}{|\mathcal{I}|/2} \sum_{\zeta\in\Gamma} \sigma_{\gamma\zeta} \left\{ \sum_{i':i_\delta=1} h_\zeta(i') - \sum_{i':i_\delta=2} h_\zeta(i') \right\}. \end{aligned}$$

It follows that all r.v.'s X_ζ such that $\zeta \notin A_\delta$ are not associated to I_δ, and therefore, if $j,k \in \mathcal{I}$ are two discrete levels such that $j_\delta = 1$, $k_\delta = 2$ and $j_{\Delta\setminus\{\delta\}} = k_{\Delta\setminus\{\delta\}}$, we have that $h_\zeta(j) = h_\zeta(k)$. Hence, for all $\zeta \notin A_\delta$, the terms $h_\zeta(i')$ from both summations cancel out and we obtain

$$\begin{aligned} a_{\delta\gamma} &= \frac{2}{|\mathcal{I}|} \sum_{\zeta\in A_\delta} \sigma_{\gamma\zeta} \left\{ \sum_{i':i_\delta=1} h_\zeta(i') - \sum_{i':i_\delta=2} h_\zeta(i') \right\} = \\ &= \frac{2}{|\mathcal{I}|} \sum_{\zeta\in A_\delta} \sigma_{\gamma\zeta} \left\{ \frac{|\mathcal{I}|}{2} \eta_\delta(1)_\gamma - \frac{|\mathcal{I}|}{2} \eta_\delta(2)_\gamma \right\} = \sum_{\zeta\in A_\delta} \sigma_{\gamma\zeta} \left\{ \eta_\delta(1)_\gamma - \eta_\delta(2)_\gamma \right\}. \end{aligned}$$

Let $\eta_{\delta\gamma} = \eta_\delta(1)_\gamma - \eta_\delta(2)_\gamma$ and the vectors $\boldsymbol{a}_{\delta A_\delta} = \{a_{\delta\gamma}\}_{\gamma\in A_\delta}$, $\boldsymbol{\eta}_{\delta A_\delta} = \{\eta_{\delta\gamma}\}_{\gamma\in A_\delta}$, $\boldsymbol{\eta}_{1A_\delta} = \{\eta_\delta(1)_\gamma\}_{\gamma\in A_\delta}$ and $\boldsymbol{\eta}_{2A_\delta} = \{\eta_\delta(2)_\gamma\}_{\gamma\in A_\delta}$. We write the matrix form of the previous expression as

$$\begin{aligned} \boldsymbol{a}_{\delta A_\delta} &= \Sigma_{\{A_\delta,A_\delta\}} \boldsymbol{\eta}_{\delta A_\delta}; \\ \boldsymbol{\eta}_{\delta A_\delta} &= \Sigma^{-1}_{\{A_\delta,A_\delta\}} \boldsymbol{a}_{\delta A_\delta}; \\ \boldsymbol{\eta}_{1A_\delta} &= \Sigma^{-1}_{\{A_\delta,A_\delta\}} \boldsymbol{a}_{\delta A_\delta} + \boldsymbol{\eta}_{2A_\delta}. \end{aligned}$$

Finally, once the values of $h_\gamma(i)$ are determined for each $\gamma \in \Gamma$, we use (5) to obtain the $\mu(i)$ values by $\mu(i) = \Sigma \cdot h(i)$. Note that although we have previously simulated a covariance matrix independently from the discrete r.v.'s, here we interpret it as a conditional covariance given the levels of $\mathcal{I}$ to generate the mean vector $\mu(i)$.

Simulation of eQTL network models of experimental crosses

We have integrated the algorithms presented above with functions from the `R/qtl` package [8] to simulate eQTL network models of experimental crosses and data from them in the following way.

First, we simulate a genetic map with a given number of chromosomes and markers using the `sim.map()` function of the `R/qtl` package. Second, we simulate a homogeneous mixed GMM in two steps: (a) we define the, possibly random, underlying regulatory model of *cis*-eQTLs, *trans*-eQTLs and gene-gene associations; (b) we simulate the parameters $(p(i), \mu(i), \Sigma(i))$ of this homogeneous mixed GMM according to the procedures described above.

Third, we simulate data from the previous eQTL network model with the function `sim.cross()` from the `R/qtl` package. This function is overloaded in `qpgraph` to plug the eQTL associations into the corresponding genetic loci and return a `R/qtl cross` object. The function `sim.cross()` defined in the `qpgraph` package proceeds as follows. First, the genotype data is simulated by the procedures implemented in the `R/qtl` package. Genotypes are sampled at each marker from a Markov chain with transition probabilities that depend on the distance between markers and a mapping function. eQTLs are placed at the markers and, in particular, if eQTLs are located sufficiently apart from each other, we can assume that the discrete r.v.'s are marginally independent between them. Finally, `qpgraph` simulates gene expression values according to the homogeneous mixed GMM by sampling continuous observations from the corresponding parameters of the CG-distribution $\mathcal{N}_{|\Gamma|}(\mu(i), \Sigma)$, given the sampled genotype i from all joint eQTLs.

An exact test of conditional independence for mixed data

The approaches to learning the structure of a mixed GMM using higher-order correlations require testing for conditional independence between any two r.v.'s X_α and X_β, such that $\beta \subseteq \Gamma$, given a set of conditioning ones X_Q, denoted as $X_\alpha \perp\!\!\!\perp X_\beta | X_Q$. To this end, we use a likelihood ratio test (LRT) between two models: a saturated model $\mathcal{M}_1$, determined by the complete graph $G^1 = (V, E^1)$, where $V = \{\alpha, \beta, Q\}$ and $E^1 = V \times V$, and a constrained model $\mathcal{M}_0$, determined by $G^0 = (V, E^0)$ with exactly one missing edge between the two vertices α, β representing the r.v.'s we wish to test, and thus $E^0 = \{V \times V\} \setminus (\alpha, \beta)$ and $Q = V \setminus \{\alpha, \beta\}$.

Note that both models are decomposable. For the model $\mathcal{M}_1$, $C_1 = V$ is the unique clique of G^1 and $S = \emptyset$ whereas for $\mathcal{M}_0$, β is always a continuous vertex, $C_1 = \{\alpha, Q\}$ and $C_2 = \{\beta, Q\}$ are the cliques of G^0 and $S = \{Q\}$ is the separator. Since $\mathcal{M}_0$ and $\mathcal{M}_1$ are decomposable, they admit explicit MLEs (Eqs. 16-18). Moreover, we restrict the

models to homogeneous mixed GMMs, in which the genotypes only affect the mean of gene expression measurements and not the variance.

Given that $V = \Delta \cup \Gamma$, we denote by (γ, ζ) a pair of continuous r.v.'s (i.e., $\gamma, \zeta \in \Gamma$), and by (δ, γ) a pair of mixed r.v.'s with $\delta \in \Delta$ and, $\gamma \in \Gamma$, so that either $Q = V \backslash \{\gamma, \zeta\}$ or $Q = V \backslash \{\delta, \gamma\}$ are the conditioning subsets.

In the context of homogeneous mixed GMMs, the null hypothesis of conditional independence for the pure continuous case, $\gamma \perp\!\!\!\perp \zeta | Q$, corresponds to a zero value in the (γ, ζ) and (ζ, γ) entries of the canonical parameter K (see Eqs. 7, 8). The log-likelihood ratio statistic, which is twice the difference of the log-likelihoods of models $\mathcal{M}_0$ and $\mathcal{M}_1$, is reduced to (see [33, pg. 192]):

$$D_{\gamma\zeta.Q} = -2 \ln \left(\frac{\mathcal{L}_0}{\mathcal{L}_1} \right) = -2 \ln \left(\frac{|ssd_\Gamma||ssd_{\Gamma \backslash \{\gamma,\zeta\}}|}{|ssd_{\Gamma \backslash \{\gamma\}}||ssd_{\Gamma \backslash \{\zeta\}}|} \right)^{n/2} = -2 \ln \left(\Lambda_{\gamma\zeta.Q} \right)^{n/2} . \tag{20}$$

The null hypothesis of conditional independence in the mixed case, $\delta \perp\!\!\!\perp \gamma | Q$, corresponds to an expansion of the canonical parameter $h_\gamma(i)$ where the terms corresponding to δ are zero, $\eta_\delta(i)_\gamma = 0$ (see Eqs. 7, 8). In this case, the log-likelihood ratio statistic is (see [33, pg. 194]):

$$D_{\delta\gamma.Q} = -2 \ln \left(\frac{|ssd_\Gamma||ssd_{\Gamma^*}(\Delta^*)|}{|ssd_{\Gamma^*}||ssd_\Gamma(\Delta^*)|} \right)^{n/2} = -2 \ln \left(\Lambda_{\delta\gamma.Q} \right)^{n/2} , \tag{21}$$

where $\Gamma^* = \Gamma \backslash \{\gamma\}$ and $\Delta^* = \Delta \backslash \{\delta\}$.

Under the null hypothesis, $D_{\gamma\zeta.Q}$ and $D_{\delta\gamma.Q}$ follow asymptotically a χ^2_{df} distribution with *df* degrees of freedom, where *df* is the difference in the number of free parameters of $\mathcal{M}_0$ and $\mathcal{M}_1$, as we shall see below.

Since models $\mathcal{M}_1$ and $\mathcal{M}_0$ are decomposable, they are collapsible onto the same set of variables $X_{V \backslash \{\gamma\}}$ (see [19, pg. 86-87], [18]). This property implies that the density functions f of $\mathcal{M}_1$ and $\mathcal{M}_0$ can be factorized as $f_V = f_{V \backslash \{\gamma\}} \cdot f_{\gamma | V \backslash \{\gamma\}}$ such that the marginal and conditional densities, $f_{V \backslash \{\gamma\}} \in \mathcal{M}_{V \backslash \{\gamma\}}$ and $f_{\gamma | V \backslash \{\gamma\}} \in \mathcal{M}_{\gamma | V \backslash \{\gamma\}}$, respectively, can be parametrized separately. Therefore, the likelihood function of $\mathcal{M}_1$ can also be computed as the product of the likelihood of the marginal and the conditional models, $\mathcal{L}_1 = \mathcal{L}^1_{\gamma | V \backslash \{\gamma\}} \cdot \mathcal{L}^1_{V \backslash \{\gamma\}}$ and, analogously, for the constrained model $\mathcal{M}_0$, $\mathcal{L}_0 = \mathcal{L}^0_{\gamma | V \backslash \{\gamma\}} \cdot \mathcal{L}^0_{V \backslash \{\gamma\}}$.

The second term of these factorizations corresponds to the same saturated model induced by the complete subgraph composed by the vertices in $V \backslash \{\gamma\}$. Then, since

$\mathcal{L}^1_{V\setminus\{\gamma\}} = \mathcal{L}^0_{V\setminus\{\gamma\}}$, we have that

$$D_{\gamma\zeta.Q} = -2\ln\left(\frac{\mathcal{L}_0}{\mathcal{L}_1}\right) = -2\ln\left(\frac{\mathcal{L}^0_{\gamma|V\setminus\{\gamma\}}}{\mathcal{L}^1_{\gamma|V\setminus\{\gamma\}}}\right) = -2\ln\left(\frac{\hat{\sigma}^0_{\gamma|V\setminus\{\gamma\}}}{\hat{\sigma}^1_{\gamma|V\setminus\{\gamma\}}}\right)^{-n/2}, \tag{22}$$

where $\hat{\sigma}^0_{\gamma|V\setminus\{\gamma\}}$ and $\hat{\sigma}^1_{\gamma|V\setminus\{\gamma\}}$ stand for the estimation of the conditional variance of the r.v. X_γ given the rest of the r.v.'s under the null and the alternative conditional models $\mathcal{M}^0_{\gamma|V\setminus\{\gamma\}}$ and $\mathcal{M}^1_{\gamma|V\setminus\{\gamma\}}$, respectively. In particular, these conditional models are equivalent to the ANCOVA models [see 19, pg. 91] in which the continuous r.v. $\gamma \in \Gamma$ is the response variable and the rest are explanatory. In this context, we have that the conditional variances in Eq. (22) are equivalent to the residual sum of squares (RSS) of the corresponding ANCOVA models divided by the sample size n, that is, $\hat{\sigma}^0_{\gamma|V\setminus\{\gamma\}} = \mathrm{RSS}_0/n$ and $\hat{\sigma}^1_{\gamma|V\setminus\{\gamma\}} = \mathrm{RSS}_1/n$.

Under the saturated model $\mathcal{M}_1$, the conditional expectation of X_γ given $X_{V\setminus\{\gamma\}}$ is

$$\mathrm{E}\left(X_\gamma|\Delta,\Gamma\setminus\{\gamma\}\right) = \alpha(i_\Delta) + \sum_{\lambda\in\Gamma\setminus\{\gamma\}} \beta_{\gamma\lambda|\Gamma\setminus\{\gamma\}} X_\lambda\,, \tag{23}$$

where $\alpha(i_\Delta) = \mu_\gamma(i_\Delta) - \sum_{\lambda\in\Gamma\setminus\{\gamma\}}\beta_{\gamma\lambda|\Gamma\setminus\{\gamma\}}\mu_\lambda(i_\Delta)$ and $\beta_{\gamma\lambda|\Gamma\setminus\{\gamma\}}$ is the partial regression coefficient that is found through the canonical parameter $K = \{k_{\gamma\zeta}\}, \forall\gamma,\zeta \in \Gamma$, as $\beta_{\gamma\lambda|\Gamma\setminus\{\gamma\}} = -k_{\gamma\lambda}/k_{\gamma\gamma}$ [33, pg. 130]. This model has $n - |\mathcal{I}| - |\Gamma| + 1$ free parameters since it has $|\mathcal{I}|$ parameters that come from the first term in Eq. (23) and $|\Gamma| - 1$ from the second term.

For the pure continuous case, the conditional expectation of X_γ given $X_{V\setminus\{\gamma\}}$ under the constrained model $\mathcal{M}_0$, is written as

$$\mathrm{E}\left(X_\gamma|\Delta,\Gamma\setminus\{\gamma,\zeta\}\right) = \alpha(i_\Delta) + \sum_{\lambda\in\Gamma\setminus\{\gamma,\zeta\}} \beta_{\gamma\lambda|\Gamma\setminus\{\gamma,\zeta\}} X_\lambda$$

which, in an analogous way as the previous case, leads to $n - |\mathcal{I}| - |\Gamma| + 2$ parameters.

By computing the difference in the number of free parameters of both models, we see that $D_{\gamma\zeta.Q}$ follows asymptotically a χ^2_{df} distribution with $df = 1$ degree of freedom.

In the mixed case, the likelihood ratio statistic $D_{\delta\gamma.Q}$ of Eq. (21) is related to the LOD score used in QTL mapping:

$$\mathrm{LOD} = \log_{10}\left(\frac{\mathcal{L}_1}{\mathcal{L}_0}\right),$$

through the following transformation of the LOD score:

$$D_{\delta\gamma.Q} = 2\ln(10)\mathrm{LOD}\,. \tag{24}$$

In fact, since the ratio between $\mathcal{L}_1$ and $\mathcal{L}_0$ is equivalent to the ratio between $\mathcal{L}^1_{\gamma|V\setminus\{\gamma\}}$ and $\mathcal{L}^0_{\gamma|V\setminus\{\gamma\}}$ we have that

$$\text{LOD} = \log_{10}\left(\frac{\mathcal{L}_1}{\mathcal{L}_0}\right) = \log_{10}\left(\frac{\mathcal{L}^1_{\gamma|V\setminus\{\gamma\}}}{\mathcal{L}^0_{\gamma|V\setminus\{\gamma\}}}\right). \tag{25}$$

In this case, the conditional expectation of the model corresponding to $\mathcal{M}_1$ is the same as the one in Eq. (23). By contrast, in the conditional expectation of the model corresponding to $\mathcal{M}_0$, we delete all the terms of Eq. (23) that involve the r.v. X_δ:

$$\mathrm{E}\left(X_\gamma|\Delta\setminus\{\delta\},\Gamma\setminus\{\gamma\}\right) = \alpha(i_{\Delta\setminus\{\delta\}}) + \sum_{\lambda\in\Gamma\setminus\{\gamma\}} \beta_{\gamma\lambda|\Gamma\setminus\{\gamma\}} X_\lambda\,. \tag{26}$$

Here, the first term involves $|\mathcal{I}_{\Delta^*}|$ parameters and the second $|\Gamma|-1$, so that the constrained model has $n-|\Gamma|-|\mathcal{I}_{\Delta^*}|+1$ free parameters. Hence, we have that $D_{\delta\gamma.Q}$, and therefore, the transformed LOD score in Eq. (24) follows a χ^2 distribution with $df = |\mathcal{I}_{\Delta^*}|(|\mathcal{I}_\delta|-1)$ degrees of freedom.

However, [33, pg. 192 to 194] observes that, for decomposable mixed GMMs, the likelihood ratios $\Lambda_{\gamma\zeta.Q}$ in Eq. (20) and $\Lambda_{\delta\gamma.Q}$ in Eq. (21) follow exactly a beta distribution. In order to enable the exact test for homogeneous mixed GMMs, we proceed to derive their corresponding parameters.

Due to the decomposability and collapsibility of the saturated $\mathcal{M}_1$ and constrained $\mathcal{M}_0$ models, we have seen that the analysis of the joint densities is equivalent to the study of the univariate conditional densities of X_γ given the rest of the variables. Concretely, for the pure continuous case, the likelihood ratio statistic $\Lambda_{\gamma\zeta.Q}$ is equivalent to the ratio $\mathrm{RSS}_1/\mathrm{RSS}_0$ where RSS_0 and RSS_1 are the residual sum of squares of the constrained and the saturated univariate models, respectively, and both follow a χ^2_k distribution, where k is the number of free parameters of each model.

Let $\mathrm{RSS}_{1.0}$ denote the difference $\mathrm{RSS}_0 - \mathrm{RSS}_1$. Following [49, pg. 166], if a r.v. X follows a χ^2_k with k degrees of freedom it also follows a gamma distribution $\Gamma(k/2,2)$. Hence,

$$\mathrm{RSS}_1 \sim \Gamma\left(\frac{n-|\Gamma|-|\mathcal{I}|+1}{2},2\right),\ \mathrm{RSS}_0 \sim \Gamma\left(\frac{n-|\Gamma|-|\mathcal{I}|+2}{2},2\right)$$

and $\mathrm{RSS}_{1.0} \sim \Gamma\left(1/2,2\right)$. Moreover, if X and Y are two independent r.v.'s such that $X\sim\Gamma\left(k_1,\theta\right)$ and $Y\sim\Gamma\left(k_2,\theta\right)$, then it can be shown [49, pg. 165] that

$$\frac{X}{X+Y} \sim \mathcal{B}(k_1,k_2)\,,$$

where $\mathcal{B}(k_1, k_2)$ denotes the beta distribution with shape parameters k_1 and k_2. Finally, if we let $X = \mathrm{RSS}_1$ and $Y = \mathrm{RSS}_{1.0}$, it follows that

$$\Lambda_{\gamma\zeta.Q} = \frac{\mathrm{RSS}_1}{\mathrm{RSS}_0} \sim \mathcal{B}\left(\frac{n - |\Gamma| - |\mathcal{I}| + 1}{2}, \frac{1}{2}\right).$$

By an argument analogous to the pure continuous case, the likelihood ratio statistic raised to the power $2/n$ for the null hypothesis of a missing mixed edge follows a beta distribution with these parameters:

$$\Lambda_{\delta\gamma.Q} \sim \mathcal{B}\left(\frac{n - |\Gamma| - |\mathcal{I}| + 1}{2}, \frac{|\mathcal{I}_{\Delta^*}|(|\mathcal{I}_\delta| - 1)}{2}\right). \tag{27}$$

This also means that the following transformation of the LOD score

$$\Lambda_{\delta\gamma.Q} = 10^{-\frac{2}{n}\mathrm{LOD}},$$

follows a beta distribution with parameters given in Eq. (27).

Note that the proportion, denoted by η^2, of (phenotypic) variance of X_γ explained by an eQTL X_δ while controlling for the rest of r.v.'s $X_{V\setminus\{\gamma\}}$, can be estimated as the difference between the estimated conditional variances of X_γ given $X_{V\setminus\{\gamma\}}$ under the saturated and the constrained models, divided by the total variance of X_γ:

$$\eta^2 = \frac{\hat{\sigma}^0_{\gamma|V\setminus\{\gamma\}} - \hat{\sigma}^1_{\gamma|V\setminus\{\gamma\}}}{\hat{\sigma}_{\gamma\gamma}} = \frac{\mathrm{RSS}_0 - \mathrm{RSS}_1}{(n-1)\cdot \mathrm{var}(X_\gamma)}. \tag{28}$$

Note that when $V\setminus\{\gamma\} = \{\delta\}$, that is, $Q = \emptyset$, the estimated conditional variance under the constrained model, RSS_0/n, is equal to the unconditional variance of X_γ ($\mathrm{RSS}_0/n = \mathrm{var}(X_\gamma)$). In this case, the proportion of the phenotypic variance explained by the eQTL reduces to [9, pg. 77],

$$\eta^2 = \frac{\mathrm{RSS}_0 - \mathrm{RSS}_1}{\mathrm{RSS}_0} = 1 - \Lambda_{\delta\gamma.Q}. \tag{29}$$

q-Order correlation graphs

The ability to test for conditional independences of arbitrary order opens up a wide spectrum of strategies that can be followed to learn a mixed GMM from data, similarly as with Gaussian GMMs for pure continuous data [see, e.g., 10, 27]. In the context of estimating eQTL networks from genetical genomics data the number of genes and genotype markers p exceeds by far the sample size n, i.e., $p \gg n$. This fact precludes conditioning directly on the rest of the genes and markers $X_{V\setminus\{i,j\}}$ when testing for an eQTL association (i, j) while adjusting for all possible indirect effects. In other words,

we cannot directly test for full-order conditional independences $X_i \perp\!\!\!\perp X_j | X_{V\setminus\{i,j\}}$.

We approach this problem using limited-order correlations, an strategy successfully applied to Gaussian GMMs [10]. It consists of testing for conditional independences of order $q < (p-2)$, i.e., $X_i \perp\!\!\!\perp X_j | X_Q$ with $|Q| = q$, expecting that many of the indirect relationships between i and j can be explained by subsets Q of size q. The extent to which this can happen depends on the sparseness of the underlying network structure G and on the number of available observations. The mathematical object that results from testing q-order correlations is called a q-order correlation graph, or qp-graph [10], and it is defined as follows.

Let P_V be a probability distribution which is Markov over an undirected graph $G = (V, E)$ with $|V| = p$ and an integer $0 \leq q \leq (p-2)$. A qp-graph of order q with respect to G is the undirected graph $G^{(q)} = (V, E^{(q)})$ where $(i,j) \notin E^{(q)}$ if and only if there exists a set $U \subseteq V\setminus\{i,j\}$ with $|U| \leq q$ such that $X_i \perp\!\!\!\perp X_j | X_U$ holds in P_V [10].

Assuming there are no additional independence restrictions in P_V than those in G, it can be shown [10] that $G \subseteq G^{(q)}$ in the sense that every edge that is present in the true underlying network G is also present in the qp-graph $G^{(q)}$. From this fact it follows that a qp-graph $G^{(q)}$ approaches G as q grows large, and therefore, $G^{(q)}$ can be seen as an approximation to G; see [10] for further details.

Because separation in undirected marked graphs with mixed discrete and continuous vertices works the same as in undirected pure graphs with either one of these two types of vertices, it follows that the definition of qp-graph also holds for mixed vertices and CG-distributions P_V.

Estimation of eQTL networks with qp-graphs

Instead of directly approaching the problem of inferring the graph structure G of the underlying eQTL network from genetical genomics data with $p \gg n$, we propose to calculate a qp-graph estimate $\hat{G}^{(q)}$. For this purpose, we use a measure of association between two r.v.'s called the *non-rejection rate* (NRR), which is defined as follows.

Let $\mathcal{Q}_{ij}^q = \{Q \subseteq V\setminus\{i,j\} : |Q| = q\}$ and let T_{ij}^q be a binary r.v. associated to the pair of vertices (i,j) that takes values from the following three-step procedure: 1) an element Q is sampled from $\mathcal{Q}_{ij}^q$ according to a (discrete) uniform distribution; 2) test the null hypothesis of conditional independence $H_0 : X_i \perp\!\!\!\perp X_j | X_Q$; and 3) if the null hypothesis H_0 is rejected then T_{ij}^q takes value 0, otherwise takes value 1.

We have that T_{ij}^q follows a Bernoulli distribution and the non-rejection rate, denoted as ν_{ij}^q, is defined as its expectancy

$$\nu_{ij}^q := \mathrm{E}[T_{ij}^q] = \Pr(T_{ij}^q = 1)\,.$$

The NRR measure was originally developed to learn qp-graphs from pure continuous data [10]. However, note that by using a suitable test for the null hypothesis $H_0 : X_i \perp\!\!\!\perp X_j | X_Q$, we can also use the NRR in mixed data sets such as those produced by genetical genomics experiments.

It can be shown [10] that the theoretical NRR is a function of the probability α of the type-I error of the test, the mean value β_{ij} of the type-II error of the test for all subsets Q, and the proportion π_{ij}^q of subsets Q of size q that separate i and j in the underlying G:

$$\nu_{ij}^q = \beta_{ij}(1 - \pi_{ij}^q) + (1 - \alpha)\pi_{ij}^q \,. \tag{30}$$

This expression helps understanding the information conveyed by the NRR in the following way. If a pair of vertices (i, j) is connected in G, then $\pi_{ij}^q = 0$ and $\nu_{ij}^q = \beta_{ij}$. This means that for associations present in G, the NRR ν_{ij}^q is 1 minus the statistical power to detect that association. In such a case, ν_{ij}^q depends on the strength of the association between X_i and X_j over all marginal distributions of size $(q + 2)$. Moreover, note that from Eq. (30) it follows that a ν_{ij}^q value close to zero implies that both, β_{ij} and π_{ij}^q, are close to zero. This means that either (i, j) is in G or q is too small.

Analogously, if ν_{ij}^q is large, then either π_{ij}^q or β_{ij} are large, and we can conclude that either (i, j) is not present in G or, otherwise, there is no sufficient statistical power to detect that association. As the statistical power to reject the null hypothesis H_0 depends on $n - q$, the latter circumstance may be due to an insufficient sample size n, a value of q that is too large, or both.

From these observations it follows that a NRR value ν_{ij}^q close to zero indicates that $(i, j) \in G^{(q)}$ while a value close to one points to the contrary, $(i, j) \notin G^{(q)}$.

The estimation of ν_{ij}^q for a pair of r.v.'s (X_i, X_j) can be obtained by testing the conditional independence $X_i \perp\!\!\!\perp X_j | X_Q$ for every $Q \in \mathcal{Q}_{ij}^q$. However, the number of subsets Q in $\mathcal{Q}_{ij}^q$ can be prohibitively large. An effective approach to address this problem [10] consists of calculating an estimate $\hat{\nu}_{ij}^q$ on the basis of a limited number subsets $Q \in \mathcal{Q}_{ij}^q$, such as one-hundred, sampled uniformly at random.

We may be interested in explicitly adjusting for confounding factors and other covariates $\mathcal{C} = \{C_1, C_2, \ldots, C_k\}$. It is straightforward to incorporate them into a NRR $\nu_{ij.\mathcal{C}}^q$ by sampling subsets Q from

$$\mathcal{Q}_{ij.\mathcal{C}}^q = \{Q \subseteq \{V \backslash \{i, j\}\} \cup \mathcal{C} : \mathcal{C} \subseteq Q \text{ and } |Q| = q\} \,.$$

Note that covariates in $\mathcal{C}$ can be known or, in the case of unknown confounding factors, estimated with algorithms such as SVA [37] or PEER [57].

Finally, the qp-graph estimate $\hat{G}^{(q)}$ of the underlying eQTL network structure G can

be obtained by selecting those edges (i, j) that meet a maximum cutoff value ϵ:

$$\hat{G}^{(q)} := \{(V, E^{(q)}) : (i, j) \in E^{(q)} \Leftrightarrow \nu_{ij}^{q} < \epsilon\}.$$

Results

Flow of genetic additive effects through gene expression

To gather insight into how mixed GMMs represent the underlying associations between genetic variants, genes and phenotypes in an eQTL network, we developed algorithms to simulate them (see Methods). These algorithms allow one to simulate mixed GMMs with given marginal correlations on the present linear associations between the genes, and given additive effects of eQTLs on their associated genes.

Using the `R/qtl` package [9] we simulated a genetic map formed by one single chromosome 100 cM long and 10 equally-spaced makers. We built an eQTL network of $p_{\Gamma} = 5$ genes forming a chain, where the first of them had one eQTL placed randomly among the ten markers (Fig. 1A). We simulated 10 mixed GMMs with the eQTL network structure shown in Figure 1A, under increasing values of the marginal correlation between the genes ($\rho = \{0.25, 0.5, 0.75\}$) and of the additive effect from the eQTL on gene 1 ($a = \{0.5, 1, 2.5, 5\}$). We sampled 1,000 data sets of $n = 100$ observations from each of these 10 models. We estimated the additive effect of the eQTL on each of the 5 genes, averaged over the 10,000 data sets at each combination of additive effect and marginal correlation. Note that only the additive effect on gene 1 is direct (Fig. 1A).

Gray lines in panels b-d of Figure 1 show the estimated average additive effects for the three different marginal correlation values on the gene-gene associations. These plots demonstrate that additive effects propagate as function of gene-gene correlations ρ. More concretely, when $\rho \geq 0.5$ moderate to large additive effects may easily show up as indirect eQTL associations when inspecting the margin of the data formed by one genetic variant and one gene expression profile. Black lines were calculated from the same data, but discarding additive effects corresponding to LOD scores below 3. This recreates the effect of selection bias [9] and shows that indirect eQTL effects are amplified under this circumstance.

The exact likelihood ratio test unlocks probing higher-order eQTL associations

Figure 1 shows that indirect additive effects in genetical genomics data can lead to spurious associations when inspecting the margin of the data formed by one gene and one

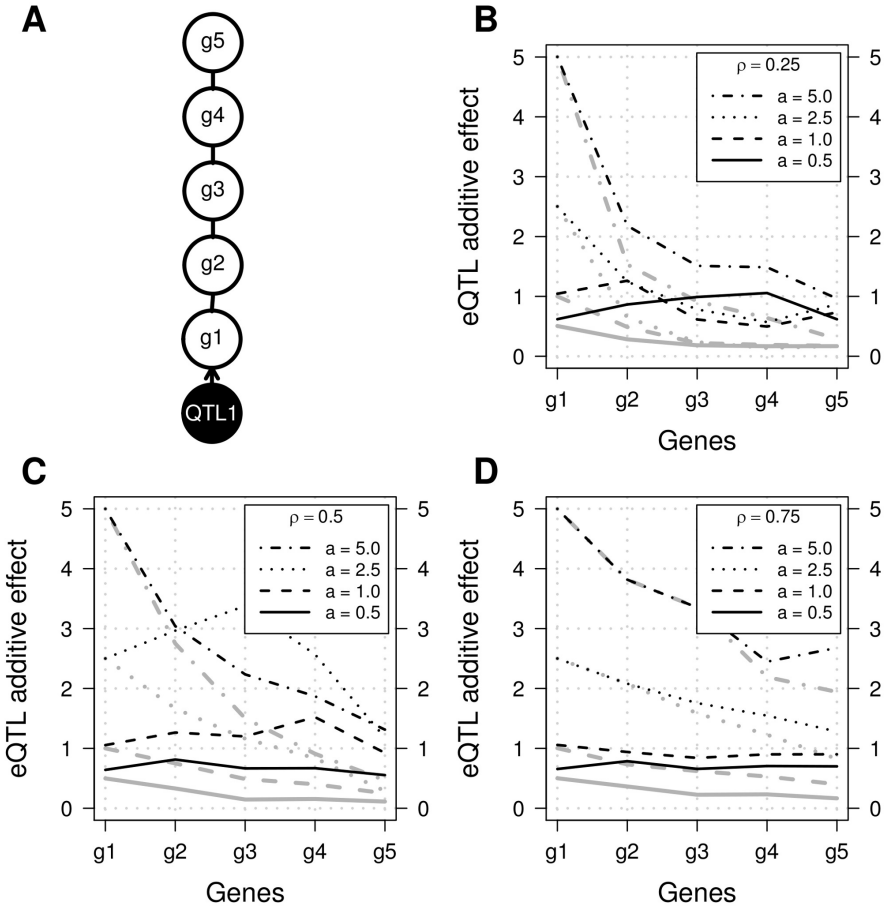

Figure 1: Propagation of indirect eQTL additive effects. Structure of the eQTL network underlying the mixed GMM employed to simulate the data shown on the other panels. All additive effects of the eQTL labeled "QTL1" on every gene g1, ..., g5, are indirect, except for g1 (A). Panels (B) to (D) show average estimated additive effects of the eQTL on each gene across 10,000 data sets simulated from different combinations of nominal gene-gene correlations (ρ) and additive effects (a). Gray lines were calculated from all data while black lines recreate the effect of selection bias by using only eQTL associations with LOD scores larger than 3.

genotype marker. More generally, when indirect effects are systematic and affect a large fraction of genes, such as batch effects [36], one also speaks of confounding effects. A classical approach to this problem within the statistical framework is to condition on the factors that confound the association of interest. In a linear regression model that treats each expression profile as a response variable and one or more markers and genes as its regressors, conditioning on confounding factors requires including them as main [e.g., 37] or mixed [e.g., 40] effects in the set of regressors.

In the context of mixed GMMs, we would like to perform a conditional independence test for mixed continuous and discrete data with conditioning sets of arbitrary size that would enable adjusting for confounding factors and for the expression of intervening

genes. In principle, this amounts to include the conditioning set as covariates in both the null and the alternative models of the likelihood ratio test (LRT) of independence for an association between a genetic marker and a Gaussian distributed phenotype. The classical resulting LOD score, which under the particular transformation shown in Eq. (24) follows asymptotically a χ^2 distribution, can be used for this purpose. However, as we shall see in this subsection, asymptotic conditions of the classical χ^2 test break under decreasing sample sizes and increasing conditioning sizes. Here we show that the exact test described in section addresses these shortcomings and enables accurately testing for higher-order conditional independence in mixed discrete and continuous data accommodating for both, linear and interaction effects between genes and genotypes.

Control of Type-I error as function of sample size

Using the same genetic map we used before, we built an eQTL network with 100 genes, where one of them, denoted g hereafter, has a *cis*-eQTL and where every gene is randomly connected to two other genes in the eQTL network in a random 2-regular graph [24]. The rest of the simulation settings were identical to the previous simulation, except that this time we considered fixed values $\rho = 0.5$ and $a = 1$, of the mean marginal correlation between the genes and of the eQTL additive effect, respectively, and different sample sizes $n = \{100, 75, 50, 25\}$.

In each data set two conditional independence tests, the asymptotic and the exact one (see Methods), were performed between the simulated genotypes from the eQTL and the simulated expression profile from a gene g' connected to g. Note that the eQTL and g' are indirectly associated by a path in the eQTL network but they are no directly connected, thereby recreating a null hypothesis of conditional independence between the eQTL and gene g' given the genes connected to g', which are g and some other gene. The asymptotic test was performed by using the `scanone()` function from the `R/qtl` package specifying the genes connected to g' as additive covariates through the `addcovar` argument. The resulting `R/qtl` LOD scores were transformed to their χ^2-distributed counterparts (see Methods). The number of rejected tests at $\alpha = 0.05$ within each sample size constitutes an estimate of the type-I error rate of the test as function of the sample size.

Figure 2A shows that as the sample size decreases the type-I error rate for the asymptotic test increases while the exact test yields a proper error rate around the nominal $\alpha = 0.05$ across all different sample sizes.

Control of Type-I error as function of network degree

We altered the previous simulation setup fixing the sample size at $n = 25$ and using eQTL networks of increasing connectivity between the genes. More concretely, we gen-

erated gene networks as random d-regular graphs [24] with $d = \{3, 4, 5, 6, 7\}$, where one of the genes g had a *cis*-eQTL. We used the same previous definition of null hypothesis, but increasing the size of the conditioning set to the d other genes connected to g', where g' is connected to g.

By counting again the number of rejected tests at $\alpha = 0.05$ across simulated data sets, we obtained the empirical type-I error rate as function of the gene network degree d, which determines the conditioning set size. Figure 2B shows that the type-I error rate grows with the degree of the underlying gene network for the asymptotic test, while the exact test controls properly the nominal level of $\alpha = 0.05$ across conditioning sets of increasing size.

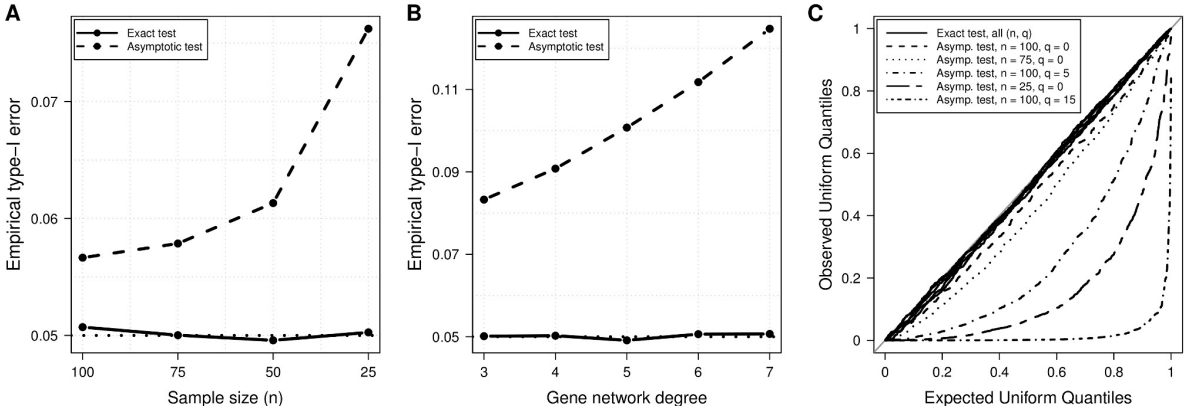

Figure 2: Empirical type-I error rate of asymptotic and exact tests for conditional independence. Plots on (A) and (B) show the empirical type-I error rate from simulated data for conditional independence tests at a nominal level $\alpha = 0.05$ (dotted horizontal line) as function of the sample size n (A), and as function of the underlying gene network degree (B). Both plots show that the exact test controls correctly the type-I error rate while the asymptotic one does not. Panel (C) contains quantile-quantile plots of Kolmogorov-Smirnov p-values obtained by testing asymptotic and exact p-values, from eQTL independence associations in a real genetical genomics yeast data set, against their expected null uniform distribution, under different sample and conditioning sizes n and q, respectively. The exact test (solid lines) produces correctly distributed null p-values while the asymptotic test displays an increasing discrepancy to the uniform distribution of null p-values as $n - q$ decreases.

Distribution of p-values under the null hypothesis

The previous two simulations revealed that the use of the LOD score in a hypothesis test for conditional independence can be problematic when taking its classical interpretation as an asymptotically distributed χ^2 statistic (Eq. 24). To assess on real data the potential impact of this observation we took a yeast genetical genomics data set [6] and explored thousands of null hypotheses of conditional independence between geno-

types and expression profiles. Under each of these null hypotheses, p-values should be uniformly distributed [38] and discrepancies to this baseline may potentially inflate the downstream rate of false discoveries after adjusting for multiple testing [37].

We recreated null hypotheses from real data by first selecting 1,000 pairs of genotype markers and gene expression profiles uniformly at random. Second, we bootstrapped 1,000 data sets by sampling with replacement a number n of observations from the original full data of 112 segregants, permuting the expression values to break any possible existing correlation between the marker and the gene.

In every bootstrapped data set, we performed a conditional independence test between each pair of marker and gene with a fixed conditioning set of q randomly chosen genes among the ones outside the 1,000 marker-gene pairs. The resulting p-value should be a *null* p-value, in the sense that it has been calculated under a simulated null hypothesis of conditional independence. We considered different combinations of sample $n = \{25, 75, 100\}$ and conditioning-order $q = \{0, 5, 15\}$ values where $q = 0$ means that we performed a hypothesis test of marginal independence. For each of these combinations of (n, q) values in a particular marker-gene pair, we assessed the goodness of fit to a uniform distribution using a Kolmogorov-Smirnov (KS) test, of the null p-values calculated from 1,000 bootstrapped data sets. In turn, as illustrated in [37], the p-values of the KS tests of the 1,000 pairs should be themselves uniformly distributed. This can be easily verified by means of quantile-quantile plots shown in Figure 2C. In these plots, uniformly distributed p-values should lead to lines close to the diagonal. This is the case for all the exact tests ran in every combination of (n, q) values, and depicted with solid lines. On the other hand, the distribution of null p-values obtained with asymptotic tests increasingly deviate from the uniform distribution as $n - q$ decreases.

Higher-order conditioning adjusts for confounding effects

Confounding effects in gene expression data affect most of the genes being profiled. Sometimes the sources of confounding are known, or can be estimated with methods such as SVA [37] or PEER [57], and may be explicitly adjusted by including them as main effects into the model. Often, however, these sources are unknown and it may be difficult to adjust or remove them without affecting the biological signal and underlying correlation structure that we want to estimate. Using simulations, here we show that confounding effects affecting all genes can be implicitly adjusted by conditioning on higher-order associations.

We used the same simulation setup as when we previously assessed type-I error rates with the following changes: (1) we did not include any association between genes; (2) the single eQTL present in the network had a fixed additive effect of $a = 2.5$; and (3) a

continuous confounding factor was included under two models with $\rho = 0.5$: a systematic one in which the confounding factor affects all genes, and a specific one in which it affects only the two genes, or the gene and maker, being tested. We considered a fixed sample size $n = 100$ and conditioning orders $q = \{0, 1, \ldots, 50\}$, where $q = 0$ corresponds to the marginal association without conditioning.

We tested for the presence of a gene-gene association and of an eQTL association between the marker containing the simulated eQTL and one of the genes not associated to that eQTL. Note that none of these associations were present in the simulated eQTL network. For every q order with $q > 0$, a subset Q of size q was sampled uniformly at random among the rest of the genes not being tested, and used for conditioning. When considering the explicit adjustment of the confounding factor, this one was added to Q except when $q = 0$ since then $Q = \{\emptyset\}$. Once Q was fixed, 100 data sets were sampled from the corresponding mixed GMM (see Methods) and two conditional independence tests were conducted in each data set for the presence of both, the eQTL and the gene-gene association, given the sampled genes in Q.

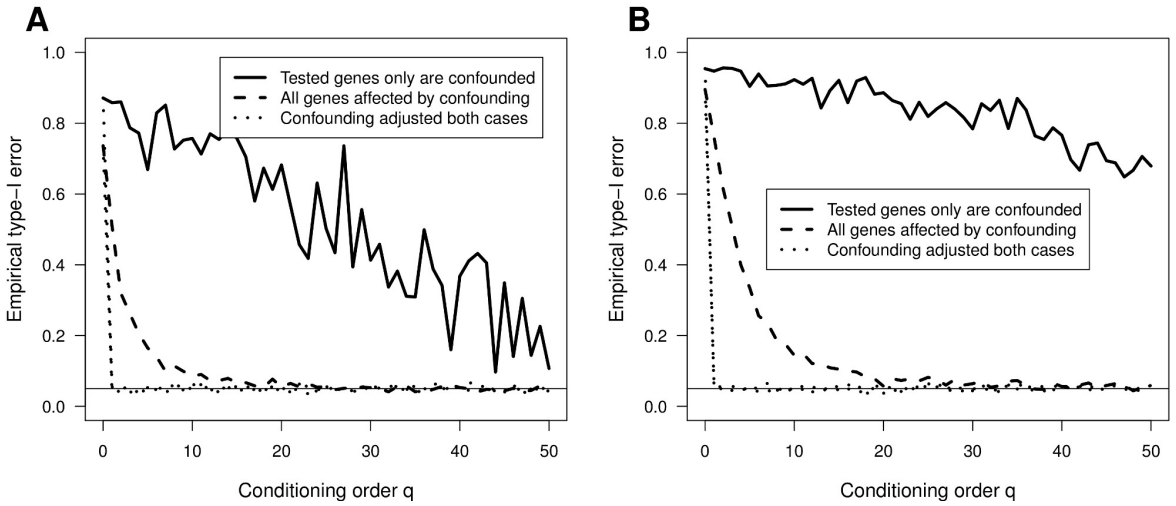

Figure 3: Explicit and implicit adjustment of confounding with higher-order conditional independence tests. Empirical type-I error rate for conditional independence tests from simulated data at a nominal level $\alpha = 0.05$ (dotted horizontal line) as function of the conditioning order q. Panel (A) shows results on testing for an absent eQTL association while panel (B) shows them for an absent gene-gene association. Solid lines correspond to the model under which confounding affects only the tested genes while dashed lines correspond to a confounding effect on all genes. In the latter situation, higher-order conditioning implicitly adjusts for the confounding effect when $q > 20$ in these data. Dotted lines from both confounding models overlap because they correspond to the inclusion of the confounding effect in the conditioning subsets, thereby explicitly adjusting for it.

Figure 3 shows the empirical type-I error rate as function of the conditioning order q,

where panel (A) corresponds to the eQTL association and (B) to the gene-gene association. This figure shows that, as expected, the explicit inclusion of the confounding factor in the conditioning subset Q (dotted lines) adjusts the confounding effect immediately with $q > 0$ in both situations, when either all genes are affected or only the tested ones. When the confounding effect is not included in Q and affects only the tested genes (solid lines), it yields high type-I error rates that only decrease linearly with $n - q$, quantity on which statistical power depends. However, when confounding affects all genes (dashed lines) the type-I error rate has an exponential decay and for $q > 20$ the confounding effect is effectively adjusted in these data.

qp-Graph estimates of eQTL networks are enriched for *cis*-acting associations

Probing higher-order eQTL associations in a genetical genomics data set can be exploited in a number of ways. One of them, described in the Methods section, consists of systematically testing for conditional independences of order q and using the expected number of non-rejections ν_{ij}^{q}, known as non-rejection rate (NRR) [10], to estimate a so-called q-order correlation graph, or qp-graph, denoted by $G^{(q)}$, as an approximation to the underlying eQTL network G.

Expression QTL acting in *cis* have more direct mechanisms of regulation than those acting in *trans* [51, 13]. This hypothesis is supported by the observation that *cis*-acting eQTLs often explain a larger fraction of expression variance, and show larger additive effects, than those acting in *trans* [51, 48, 13]. On the other hand, spurious eQTL associations tend to inflate the discovery of *trans*-acting eQTLs [5]. From this perspective, it makes sense to expect an enrichment of *cis*-eQTLs when indirect associations are effectively discarded [29, 40].

We estimated NRR values ν_{ij}^{q} on every pair (i, j) of marker and gene from the yeast data set of $n = 112$ segregants for different $q = \{25, 50, 75, 100\}$ orders, restricting conditioning subsets to be formed by genes only. The resulting estimates $\hat{\nu}_{ij}^{q_k}, q_k \in q$, were averaged, $\hat{\nu}_{ij}^{\bar{q}} = \frac{1}{|q|} \sum_{q_k} \hat{\nu}_{ij}^{q_k}$, to account for the uncertainty in the choice of the conditioning order q [11].

We ranked marker-gene pairs (i, j) by average NRR values $\hat{\nu}_{ij}^{\bar{q}}$ and made a comparison against the ranking by p-value of the (exact) LRT for marginal independence (i.e., where $q = 0$) to directly assess the added value of higher-order conditioning under the same type of statistical test. We considered conservative and liberal cutoff values $\epsilon = \{0.1, 0.5\}$ on the average NRR $\hat{\nu}_{ij}^{\bar{q}}$ and obtained two different qp-graph estimates of the underlying eQTL network, denoted by $\hat{G}_{\epsilon}^{(\bar{q})} = (V, E_{\epsilon}^{(\bar{q})})$, each of them having $|E_{0.1}^{(\bar{q})}| = 4,667$ and

$|E^{(\bar{q})}_{0.5}| = 81,360$ edges.

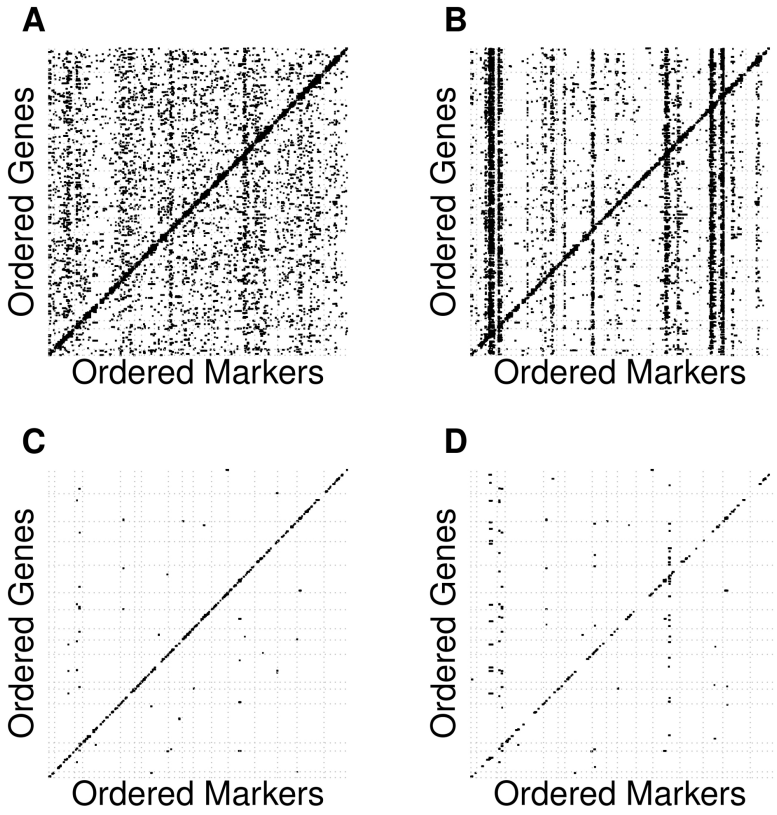

Figure 4: Enrichment of *cis*-acting eQTL associations. Dot plots of eQTL associations in yeast, where the x-axis and y-axis represent positions along the genome of markers and genes, respectively. Diagonal bands arise from *cis*-eQTLs while vertical ones from *trans*-eQTLs. Each row shows the top-k eQTLs with largest strength in terms of non-rejection rates (A, C) and p-values for the null hypothesis of marginal independence (B, D), where k was the number of eQTLs meeting a liberal (A) and conservative (C) cutoff on the non-rejection rate. Hence, panels in each row contain the same number of eQTLs. Conditioning with the approach introduced in this paper (A, C) leads to more *cis*-acting eQTLs than using marginal tests (B, D); see Table 1.

We then selected the top-k number of marker-gene pairs (i, j) with lowest p-value in the marginal independence test, where $k = \{|E^{(\bar{q})}_{\epsilon}|\}$, which led to two other estimates of the eQTL network, denoted by $\hat{G}^{(0)}_{\epsilon}$. Note that both, $\hat{G}^{(\bar{q})}_{\epsilon}$ and $\hat{G}^{(0)}_{\epsilon}$, have the same number of edges, in this case, pairs (i, j) of eQTL associations between a marker and a gene, thereby enabling a direct comparison of the fraction of *cis* and *trans*-acting selected eQTL associations.

In Figure 4 we can see dot plots of the eQTL associations present in qp-graphs $\hat{G}^{(\bar{q})}_{\epsilon}$ (panels A, C), and those present in $\hat{G}^{(0)}_{\epsilon}$ by using the marginal approach (panels B, D). Given the same number of eQTL associations, Figure 4 shows that qp-graph estimates of the underlying eQTL network have a higher number of *cis*-acting eQTLs, with an increase

Table 1: Enrichment of *cis*-eQTL associations. Number of *cis*-eQTL associations in yeast found by the method introduced in this paper (qp-graph) and by a marginal test of independence, indicated as row names. The third row reports the enrichment of *cis*-eQTLs of qp-graph over the marginal approach. Different columns correspond to different cutoffs (conservative, liberal) employed by qp-graph to select eQTLs and different distances (500bp and 10kb) around genes to call eQTL as *cis*-acting. Using higher-order conditional independences (qp-graph) yields between 26% and 58% more *cis*-eQTL associations in the yeast data set, depending on the minimum strength of eQTLs and their maximum distance to their associated genes.

	Conservative cutoff (4,667 eQTLs)		**Liberal cutoff** (81,360 eQTLs)	
Method	***cis* dist. 500bp**	***cis* dist. 10kb**	***cis* dist. 500bp**	***cis* dist. 10kb**
qp-graph	278	1,998	911	8897
marginal	221	1,367	646	5626
Enrichment	26%	46%	41%	58%

between 25% to 58% over the marginal test (see Table 1). Moreover, with the marginal approach many more vertical bands of *trans*-acting associations remained present among the strongest selected eQTLs (panel D), than with the qp-graph estimate (panel C). We interpret this observation as evidence of the propagation of additive effects due to strong gene-gene correlations either present in the underlying eQTL network or created by confounding effects, and possibly aggravated by selection bias, as previously shown in Figure 1.

Higher-order conditioning leads to sparser eQTL networks with more direct *trans*-acting associations

Gene expression is often influenced by several *trans*-acting regulators. The genetic variability associated to each of these regulators normally makes a small contribution to the overall genetic effect that modulates the transcriptional throughput of the target gene [13]. This makes it even harder to find genuine direct *trans*-acting eQTLs because small additive effects may also result from the propagation of large effects through gene-gene correlations and selection bias (see Fig. 1).

We explored the use of higher-order conditioning to filter out spurious *trans*-acting eQTLs selected by classical QTL mapping with LOD scores. To this end, we first conducted single marker regression analysis with the `R/qtl` package [9] to identify *trans*-eQTLs located at least 500bp away from the linked gene. Using permutation tests from

`R/qtl`, p-values were calculated and 31,478 eQTLs met a genome-wide cutoff of $p < 0.01$, corresponding to a genome-wide minimum LOD score of 4.32. Among these eQTLs, 535 were *cis*-acting and the remaining *trans*-eQTLs were associated to 2,416 different genes. Note that this estimate of the eQTL network corresponds to a qp-graph estimate with $q = 0$, $\hat{G}^{(0)}$, based on a permutation test with a null hypothesis for each gene of no eQTL anywhere in the genome.

Using average NRR estimates $\hat{\nu}_{ij}^{\bar{q}}$ calculated in the previous subsection and a conservative cutoff value of $\epsilon = 0.1$, we selected a qp-graph estimate $\hat{G}_{0.1}^{(\bar{q})} \subseteq \hat{G}^{(0)}$ which only had 361 genes with at least one *trans*-eQTL, from the initial set of 2,416. Recall from previous sections, that this means that for each eQTL in $\hat{G}_{0.1}^{(\bar{q})}$, on average through the different $q = \{25, 50, 75, 100\}$, at least 90% of LRTs reject the null hypothesis of q-order conditional independence.

Among the 361 genes in $\hat{G}_{0.1}^{(\bar{q})}$ with at least one *trans*-eQTL, only 12 had exactly the same eQTLs in the initial estimate $\hat{G}^{(0)}$ obtained by single marker regression. For each of the remaining 349, we compared the following two linear models with the expression profile of each gene, denoted by Y_γ, as response variable and the linked *trans*-acting eQTLs, denoted by $I_1, \ldots, I_l$, as explanatory factors:

$$\begin{aligned} H_1: \quad Y_\gamma &= \beta_0 + \beta_1 I_1 + \cdots + \beta_k I_k + \beta_{k+1} I_{k+1} + \cdots + \beta_l I_l + \epsilon\,, \\ H_0: \quad Y_\gamma &= \beta_0 + \beta_1 I_1 + \cdots + \beta_k I_k + \epsilon\,. \end{aligned}$$

Since the linear models derived from $\hat{G}_{0.1}^{(\bar{q})}$, and corresponding to H_0, are nested into those derived from $\hat{G}^{(0)}$, we can test for each gene Y_γ whether the models from $\hat{G}^{(0)}$ explain a significantly larger amount of variance than the ones from $\hat{G}_{0.1}^{(\bar{q})}$ using an F-test.

Figure 5A shows the distribution of the resulting 349 p-values. For the vast majority of them (83% with $p > 0.05$) we cannot reject the null hypothesis at a reasonable significance level, and therefore, the sparser model derived from the qp-graph $\hat{G}_{0.1}^{(\bar{q})}$ should be preferred. We repeated again this exercise replacing the eQTLs in each gene from $\hat{G}_{0.1}^{(\bar{q})}$ by randomly chosen ones among those that form part of the larger model for the same gene in $\hat{G}^{(0)}$. The result, in Figure 5B, reveals that in comparison with the eQTLs selected in $\hat{G}_{0.1}^{(\bar{q})}$, fewer of the null (random) models (57% with $p > 0.05$) fit the data as good as the alternative larger models. Note that these null random models are still built with eQTLs significantly linked to their gene by single marker regression, which may explain a substantial fraction of the gene expression variability in the 43% of the models with $p < 0.05$. These are likely to be conservative estimates of the fraction of sparser models that are more consistent with the data since we are not correcting p-values for multiple testing.

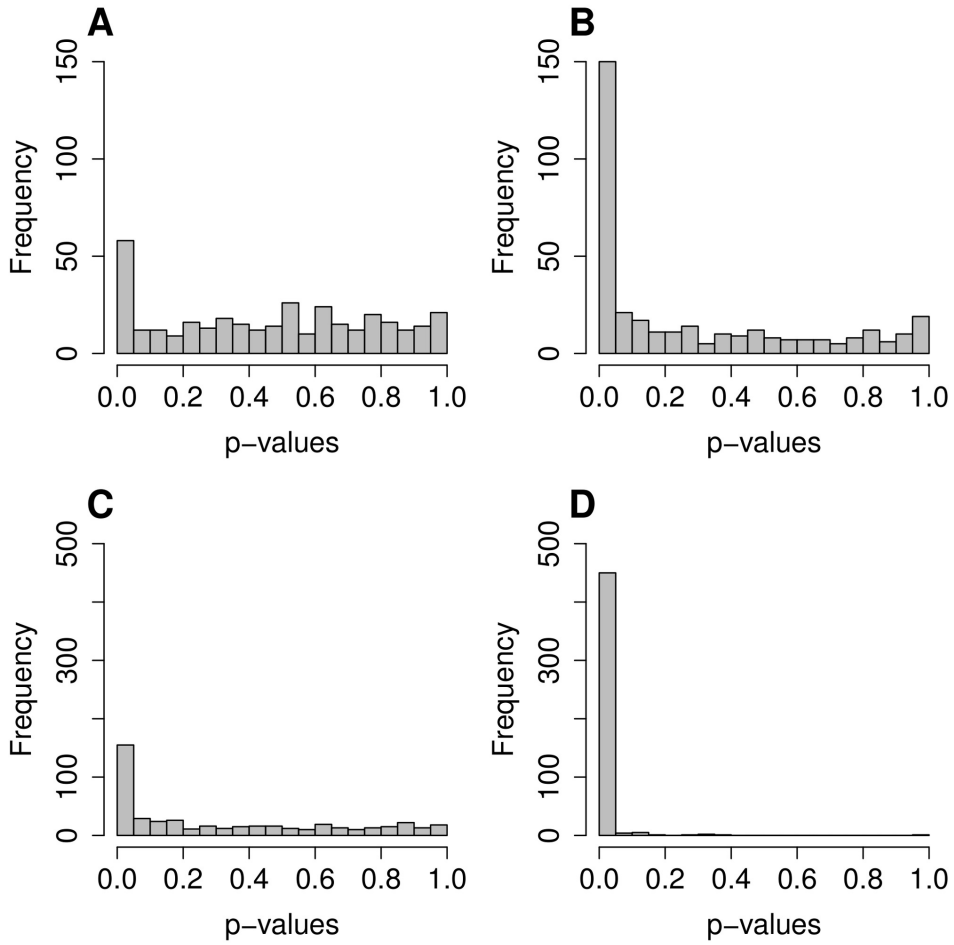

Figure 5: Fit of gene models with *trans*-eQTLs to yeast data. Distribution of p-values for the F-test between sparser qp-graph $\hat{G}^{(\bar{q})}_{0.1}$ (null) models and larger single marker (alternative) models. Null qp-graph models were derived from genes γ with *trans*-eQTLs δ located at a minimum distance of 500bp from the target gene, and found significant by single marker regression at a genome-wide $p < 0.01$ and discarding those with NRR $\hat{\nu}^{\bar{q}}_{\gamma\delta} > 0.1$. Panel (A) contains p-values from 349 genes with at least one *trans*-eQTL in $\hat{G}^{(\bar{q})}_{0.1}$. Panel (B) results from using the same alternative $\hat{G}^{(0)}$ models as in (A) but replacing eQTLs δ in null models by different ones δ' randomly selected among those in the alternative models. Panel (C) contains p-values from 465 genes γ with no *trans*-eQTLs in $\hat{G}^{(\bar{q})}_{0.1}$ but connected to at least one other gene in $\hat{G}^{(\bar{q})}_{0.1}$. In this case, genes η in $\hat{G}^{(\bar{q})}_{0.1}$ whose $\hat{\nu}^{\bar{q}}_{\gamma\eta} < 0.1$ where included in both, the null and the alternative models. Panel (D) results from using the same alternative $\hat{G}^{(0)}$ models as in (C) but replacing genes η in null models by different ones η' randomly selected among the rest of the genes in the data set. The vast majority of tests in (A, C) have $p > 0.05$, thus indicating that denser alternative gene models derived from single marker regression $\hat{G}^{(0)}$ do not fit the data significantly better than the sparser null models derived from qp-graph estimates $\hat{G}^{(\bar{q})}_{0.1}$. This fact changes substantially in the control experiments shown in (B, D).

The qp-graph estimate $\hat{G}^{(\bar{q})}_{0.1}$ had 2,055 genes for which all their *trans*-acting eQTLs were removed from the initial $\hat{G}^{(0)}$. This means that at least 10% of higher-order conditional independence tests could not reject the null hypothesis between every of these 2,055 genes and any of the *trans*-eQTLs significantly linked to them by single marker regression at a genome-wide $p < 0.01$. The explanation for this discrepancy is that conditioning on the rest of genes, the linked eQTLs do not explain a significantly larger fraction of the variability of the target gene. We verified this hypothesis using an analogous strategy to the previous case on the 349 genes. However, this time we could only consider the fraction of the 2,055 eQTL genes (465/2,055) that had at least one gene-gene association in $\hat{G}^{(\bar{q})}_{0.1}$. For every of these 465 genes, we added to the null and alternative models, those genes $Y_1, \ldots, Y_k$ in $\hat{G}^{(\bar{q})}_{0.1}$ connected to the target gene Y_γ, i.e., with $\hat{\nu}_{\gamma j} < 0.1, j = 1, \ldots, k$:

$$
\begin{aligned}
H_1: \quad Y_\gamma &= \beta_0 + \beta_1 Y_1 + \cdots + \beta_k Y_k + \beta_{k+1} I_{k+1} + \cdots + \beta_l I_l + \epsilon\,, \\
H_0: \quad Y_\gamma &= \beta_0 + \beta_1 Y_1 + \cdots + \beta_k Y_k + \epsilon\,.
\end{aligned}
$$

Figure 5C shows the distribution of p-values of the F-test between these two models and 67% of them had $p > 0.05$. We performed an analogous control to the one used before, this time replacing the genes $Y_1, \ldots, Y_k$ by randomly select ones among the rest in the data set. The resulting p-value distribution shown in Figure 5D reveals that most of tests could be rejected, and therefore, the *trans*-eQTLs identified by single marker regression do explain a significantly larger fraction of the variability of the target gene, than just using gene expression from randomly selected genes. A larger *cis*-region of 10Kb gives similar results (Supplementary Fig. S1).

The striking differences in Figure 5 between panels (A, C) and (B, D) confirm, from a purely statistical standpoint, that higher-order conditioning can effectively help to discard indirect *trans*-acting eQTL associations. However, they tell little about differences in biological information conveyed by sparser eQTL network estimates which, *a priori*, fit the data better.

We attempted to address this question in a systematic way by adapting an approach previously used with transcriptional networks [11] for this same purpose. This approach estimates the degree of coherence between the biological function of a transcription-factor coding gene and its putative targets using Gene Ontology (GO) annotations [1]. This degree of functional coherence (FC) takes values between 0 and 1, where 1 implies identical biological function and 0 completely different. Assuming genes acting closer in a pathway should exert more similar functions than those acting far apart, one should expect that FC estimates of direct associations are closer to 1 than those calculated from

indirect ones.

To enable this kind of analysis with eQTL associations we restricted it to those overlapping a gene and assumed that the GO terms of this gene describe the functions most directly affected by the genetic variability of the eQTL. We also fetched the GO terms of the gene *trans*-associated to the eQTL. Finally, an FC estimate for each *trans*-eQTL was obtained by comparing the GO term hierarchy growing at the terms annotated to the eQTL-overlapping gene with the one growing at the terms annotated to the target gene. The comparison was performed by calculating the ratio between the intersection of GO terms between the two hierarchies divided by their union [11]. Note that GO annotations themselves are partial and, in some cases, inaccurate but one may expect that the large number of available annotations for an organism such as yeast still enable this approach.

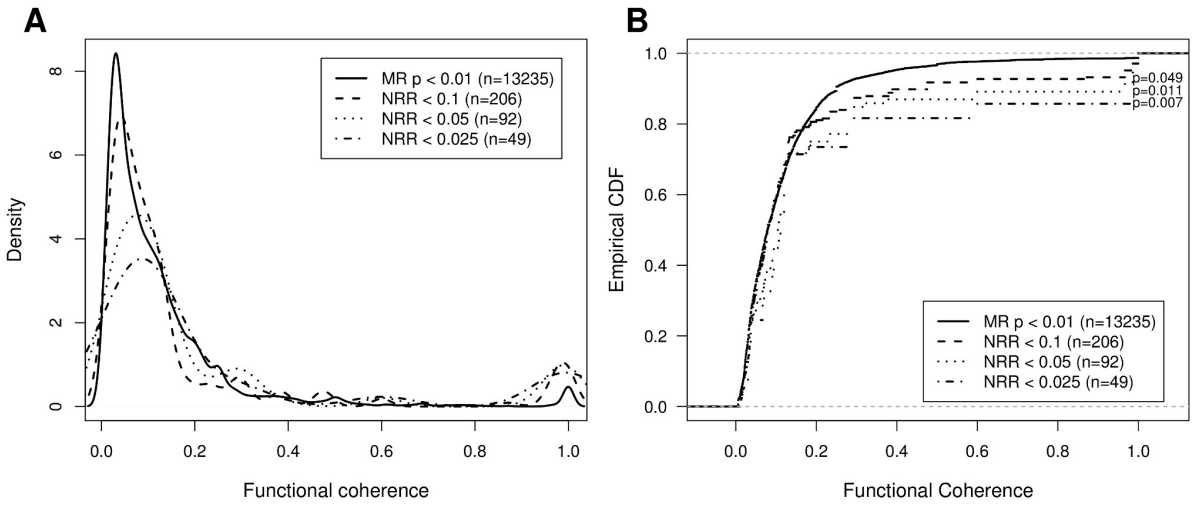

Figure 6: Functional coherence of *trans*-eQTLs. Densities (A) and empirical cumulative distribution functions -CDFs- (B) of estimated values of functional coherence (FC) of *trans*-acting eQTL associations selected by single marker regression (MR) at a genome-wide $p < 0.01$ and by different cutoffs of the non-rejection rate -NRR- (0.1, 0.05, 0.025). The legend indicates the number n of eQTLs for which FC could be estimated. In panel (B), at the height of each line for FC=0.8, the p-value for the Kolmogorov-Smirnov (KS) test on whether the corresponding CDF of NRR values is stochastically larger than the one of MR values, is reported. It follows that FC values increase significantly ($p < 0.05$) when restricting MR *trans*-eQTL associations to those selected by NRR and higher-order conditioning.

We proceeded to calculate FC values on *trans*-eQTLs from the eQTL network estimated by single marker regression with genome-wide $p < 0.01$, $\hat{G}^{(0)}$, and from qp-graph estimates derived from three different NRR cutoffs, $\hat{G}^{(\bar{q})}_{0.1}, \hat{G}^{(\bar{q})}_{0.05}, \hat{G}^{(\bar{q})}_{0.025}$. To avoid having results depending on the minimum distance employed to call an eQTL as *trans*-acting, we focused the analysis on those eQTLs whose target genes were located in a different chromosome.

Figure 6 shows the densities and empirical cumulative distribution functions (ECDF) of FC values from each eQTL network estimate. It can be seen that as the NRR cutoff decreases, the FC distribution shifts towards larger values. This shift is significant with respect to the single marker regression estimate, when testing the difference in ECDFs by a Kolmogorov-Smirnov test ($p < 0.05$). This implies that larger fractions of rejected conditional independence tests lead to larger FC values which, in turn, suggest that eQTLs with small (stronger) NRR values are in some sense functionally "closer" to the target gene than eQTLs with weaker (larger) NRR values. From the statistical and biological evidence provided in this subsection we may conclude that higher-order conditioning leads to sparser eQTL networks with more direct *trans*-acting associations.

The genetic control of a gene expression network in a yeast experimental cross

We took a closer look to the qp-graph estimate $\hat{G}_{0.1}^{(\bar{q})}$ of the yeast eQTL network. First, we focused on the genetic connected components involving at least one *cis* or *trans*-acting eQTL association. These components involved 379 genes and 288 eQTLs, with a median of 4 eQTls per gene. A significant percentage of genes (20%) had more than 10 eQTLs on the same chromosome of the linked gene. Since eQTLs in $\hat{G}_{0.1}^{(\bar{q})}$ were independently mapped from each other, a fraction of those targeting a common gene may be tagging the same causal variant. We removed redundant eQTLs by the following forward selection procedure. For each gene, we ordered its linked eQTLs by increasing NRR values $\nu_{ij}^{(\bar{q})}$ and proceeded over the ranked eQTLs to test the conditional independence of the gene and the eQTL, given the eQTLs occurring before in the ranking. An eQTL association was retained if the test was rejected at $p < 0.05$ and the selection procedure stopped whenever $p > 0.05$ to continue on the next gene.

The genetic connected components were substantially pruned and the vast majority of genes (328/379) were left with just one eQTL, 50 genes with two, and only one gene had 3 eQTLs. This final eQTL network comprised 288 eQTLs and 1,295 genes, the vast majority of them (916) forming gene-gene associations without any eQTL.

The larger genetic effects are *trans*-acting on hub genes

Using the previous forward selection strategy, this time without testing and dropping any eQTL, we applied Eq. (28) to each of the 379 genes with at least one eQTL the to estimate the percentage of variance explained by eQTLs at each gene, adjusting for the presence of multiple eQTLs in the case of the 51 genes with more than one. The distribution of resulting values is shown in Figure 7A. About half of the genes had eQTLs

explaining 50% or less of their expression variability, and only in about 10% their eQTLs explained more than 70% of it. The small fraction of genes (6%) with eQTLs explaining less than 20% of their variance is consistent with the adjustment of small effects due to indirect associations (Fig. 1).

Using a method based on linear mixed modeling and exploiting the relatedness matrix built from all pairs of segregants [35, 4] we estimated the narrow-sense heritability h^2 for these 379 genes and compared it against the percentage of variance explained by the eQTLs (Fig. 7B). Setting the percentage explained to the expected maximum h^2 when the former was larger, the fraction of missing heritability ranges from 0 to 73%. We labeled genes in this figure by their connectivity degree to other genes in the eQTL network. We observed that this degree correlated positively with both, h^2 and percentage of variance explained. In fact, as Figure 7C shows, genes whose eQTLs explained more than 70% of their variability, were connected to 9 or more other genes in the eQTL network. This means that, in this case, the larger genetic control on gene expression takes place on those genes acting as hubs in the network. Interestingly, labeling these genes with the distance to their eQTL reveals that most of them have a *trans*-acting eQTL located in a different chromosome. In fact, these particular *trans*-eQTLs map all of them to chromosomes II and III (Table 2). Concretely, genes *DSE1*, *SCW11*, *DSE2* are associated to the same marker in chromosome II which is located less than 1kb from the *AMN1* gene. This gene carries a loss-of-function mutation in the BY strain [60] affecting the expression of daughter cell-specific genes. The eQTLs in chromosome III map to the MAT and LEU2 loci, the latter being one of the engineered deletions in the BY strain. For two of the genes, *YLR040C* and *YCR097W-A*, their functions are unknown, but a Gene Ontology (GO) enrichment analysis among the genes connected to them in the eQTL network shows that they are likely to be involved in mating-specific regulatory processes (Supplementary Tables S1 and S2).

Therefore, the highly-connected genes, shown in Table 2, are involved in regulatory processes related to mating-specific expression, reacting upon nitrogen starvation, participation in the leucine biosynthesis pathway and daughter cell separation. These are fundamental pathways for yeast growth and render these results consistent with previous evidence from yeast genetic interaction networks derived from double-mutant screens [16], where highly-connected genes were involved in primary cellular functions [2].

Differential genetic control of gene expression across chromosomes

We also investigated how genetic variation affects gene expression differently across the yeast chromosomes. For this purpose, we produced hive plots [32], one for each chromosome, shown in Figure 8. A first observation is that eQTLs occurring within

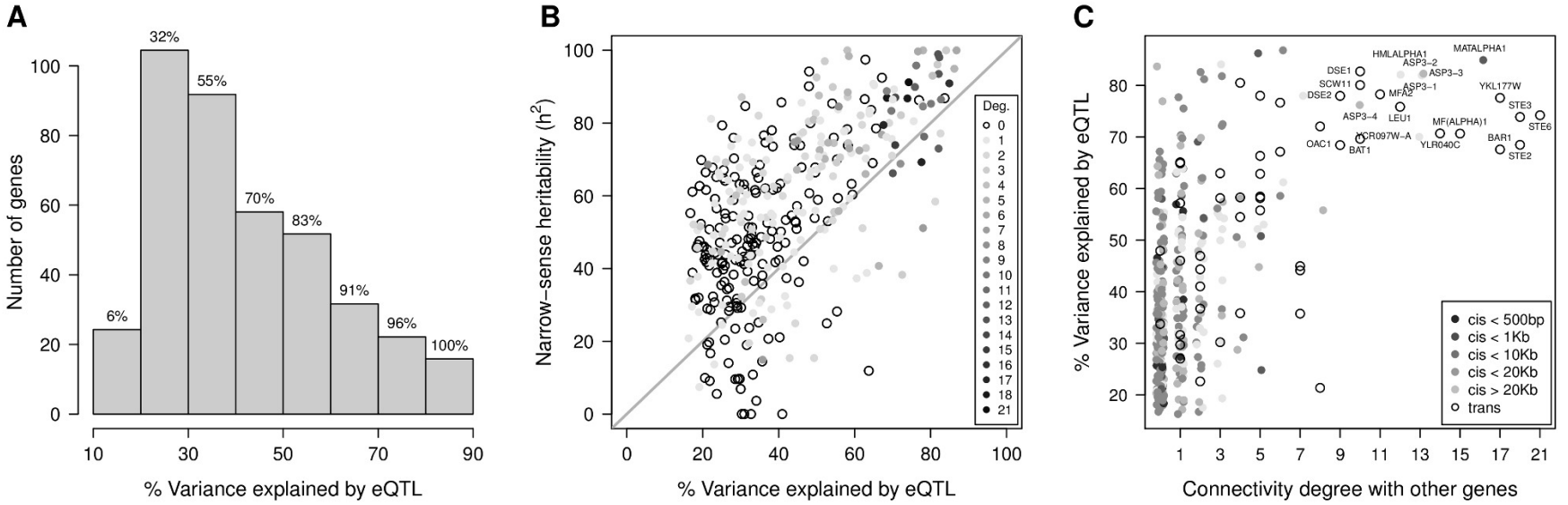

Figure 7: Variance explained in the eQTL network. (A) Distribution of the percentage of gene expression variance explained by eQTLs. The cumulative percentage of genes is reported on top of each bar. A majority of genes has eQTLs that together explain less than 40% of the expression variance. Only about 10% of the genes have eQTLs that explain more than 70% of their expression variance. (B) Scatter plot of the narrow-sense heritability h^2 as function of the percentage of variance explained by eQTLs. The diagonal line is drawn at values where this percentage equals h^2, and it is only shown as a visual guide. Open circles correspond to genes with exclusively eQTL associations while solid ones indicate also the presence of at least one association to other gene. The gray scale in solid circles correlates with the connectivity degree of gene-gene associations in the eQTL network, as indicated in the legend. Both, h^2 and variance explained by eQTLs, is higher for genes with more gene-gene associations. (C) Percentage of variance explained by eQTLs as function of the connectivity degree with other genes in the eQTL network. Degrees 19 and 20 had no genes and are omitted from the x-axis. Genes whose eQTLs explain more than 70% of their expression variance are connected to at least 9 other genes in the eQTL network. The gray scale indicates distance to the eQTL, which was averaged when a gene had more than one and is darker for closer distances. An open circle indicates an eQTL in a chromosome different to the one of the gene, denoted as *trans* in the legend.

Table 2: Genes with more than 70% variance explained. Genes whose eQTLs explain 70% or more of their expression variance. The column "Pathway" specifies the primary pathway or molecular process in which the gene is involved, where "(pr.)" indicates that the gene has unknown function and its pathway has been predicted using the eQTL network. The abbreviations correspond to mating-specific expression or related regulation (Mating Reg.), nitrogen starvation (Nitr. starvation), leucine biosynthesis (Leu biosynthesis), and in daughter cell separation (Daught. cell sep.). All genes had one single eQTL and the column location reports whether the eQTL occurs in the same chromosome of the gene (*cis*) or in a different one *trans*. When the eQTL is classified as *cis*, its distance to the gene is reported in column "Dst.". Columns h^2 and η^2 report, respectively, the narrow-sense heritability and the fraction of variance explained by the eQTL. The column "Deg." (degree) gives the number of genes associated in the estimated eQTL network.

Gene	**Chr**	**Pathway**	**Location**	**Dst. (bp)**	h^2	η^2	**Deg.**
STE6	XI	Mating reg.	trans (III)	NA	0.91	0.74	21
STE2	VI	Mating reg.	trans (III)	NA	0.87	0.69	18
STE3	XI	Mating reg.	trans (III)	NA	0.87	0.74	18
BAR1	IX	Mating reg.	trans (III)	NA	0.79	0.68	17
YKL177W	XI	Mating reg.	trans (III)	NA	0.69	0.78	17
MATALPHA1	III	Mating reg.	cis (III)	732	0.91	0.85	16
MF(ALPHA)1	XVI	Mating reg.	trans (III)	NA	0.74	0.71	15
YLR040C	XII	Mating reg. (pr.)	trans (III)	NA	0.87	0.71	14
YCR097W-A	III	Mating reg. (pr.)	cis (III)	118,623	0.66	0.70	13
ASP3-1	XII	Nitr. starvation	cis (XII)	31,174	0.99	0.82	13
ASP3-2	XII	Nitr. starvation	cis (XII)	27,522	0.94	0.82	13
ASP3-3	XII	Nitr. starvation	cis (XII)	17,942	0.98	0.82	13
HMLALPHA1	III	Mating reg.	cis (III)	187,892	0.73	0.82	12
LEU1	VII	Leu biosynthesis	trans (III)	NA	0.90	0.76	12
MFA2	XIV	Mating reg.	trans (III)	NA	0.76	0.78	11
DSE1	V	Daugh. cell sep.	trans (II)	NA	0.86	0.83	10
SCW11	VII	Daugh. cell sep.	trans (II)	NA	0.85	0.80	10
BAT1	VIII	Leu biosynthesis	trans (III)	NA	0.83	0.70	10
ASP3-4	XII	Nitr. starvation	cis (XII)	14,290	0.96	0.76	10
DSE2	VIII	Daugh. cell sep.	trans (II)	NA	0.85	0.78	9
OAC1	XI	Leu biosynthesis	trans (III)	NA	0.89	0.68	9

the same chromosome (edges between the markers and *cis*-genes axes) mostly lead to concentric edges, pointing to *cis* regulatory mechanisms acting at different distances. A remarkable exception is chromosome III where many of those edges cross through each other. This chromosome is also distinctive in that it has a lower density of *cis*-acting eQTLs than the rest of the genome.

At 100 kb from the beginning of chromosome III there is a *cis*-acting eQTL on gene *LEU2*. This eQTL is also *trans*-associated to the genes *BAT1*, *OAC1*, *LEU1* and *BAP2* involved in the leucine biosynthesis pathway. According to the UCSC Genome Browser (`http://genome.ucsc.edu`) they all have upstream a binding site of *LEU3*, a major regulatory switch in this pathway. The engineered deletion of *LEU2* affects *LEU3* in a feedback loop and this would lead to expression changes in its targets [46, 14].

Downstream, at about 200 kb of the beginning of chromosome III, we find the *MAT* locus whose genetic composition determines the mating type of yeast. This eQTL is *cis*-associated to the gene *MATALPHA1* which is expressed in haploids of the alpha mating type and which has been previously reported as a candidate regulator of the rest of genes associated to this locus [60, 17]. This locus is *trans*-associated to two other genes in the same chromosome (*HMLALPHA1*, *HMRA1*) and to a set of genes distributed throughout the genome (*STE2*, *STE3*, *STE6*, *AFB1*, *BAR1*, *MF(ALPHA)1*, *MFA2*) which are all involved in the regulation of mating-type specific transcription.

In chromosome V, around the locus of *URA3* we find a *cis*-acting eQTL which as a *trans*-acting effect on *URA1* (chromosome XI) and *URA4* (chromosome XII), the three of them taking part in the biosynthesis of pyrimidines [60, 17]. As it can be easily seen from Figure 8, and consistent with previous observations [60], few of the eQTLs affect directly transcription factors, such as the *ARR1* gene in chromosome XI, or RNA-binding proteins, such as *NOP8* in chromosome V.

The edges between the *cis*-genes and the *trans*-genes axes, correspond to gene-gene associations from the corresponding chromosome to the rest of the genome and where at least one of the genes has an eQTL. This is a fraction (431) of a total of 2,048 gene-gene associations on the entire eQTL network, more directly affected by the genetic control of gene expression. We observed a systematic pattern of association between genes from the same chromosome. Replacing the *trans*-genes axis of the entire genome by another axis again of the same chromosome (Supplementary Fig. S2) reveals that a fraction of the gene-gene associations in which one of the genes has a *cis*-acting eQTL, occur between genes close to each other on the chromosome. It may be possible that inherited co-expression segregates due to linkage disequilibrium and/or that tandem gene duplication events render genes close to each other being co-expressed. Using further the strategies introduced in this paper, such as conditioning these associations on nearby genes may

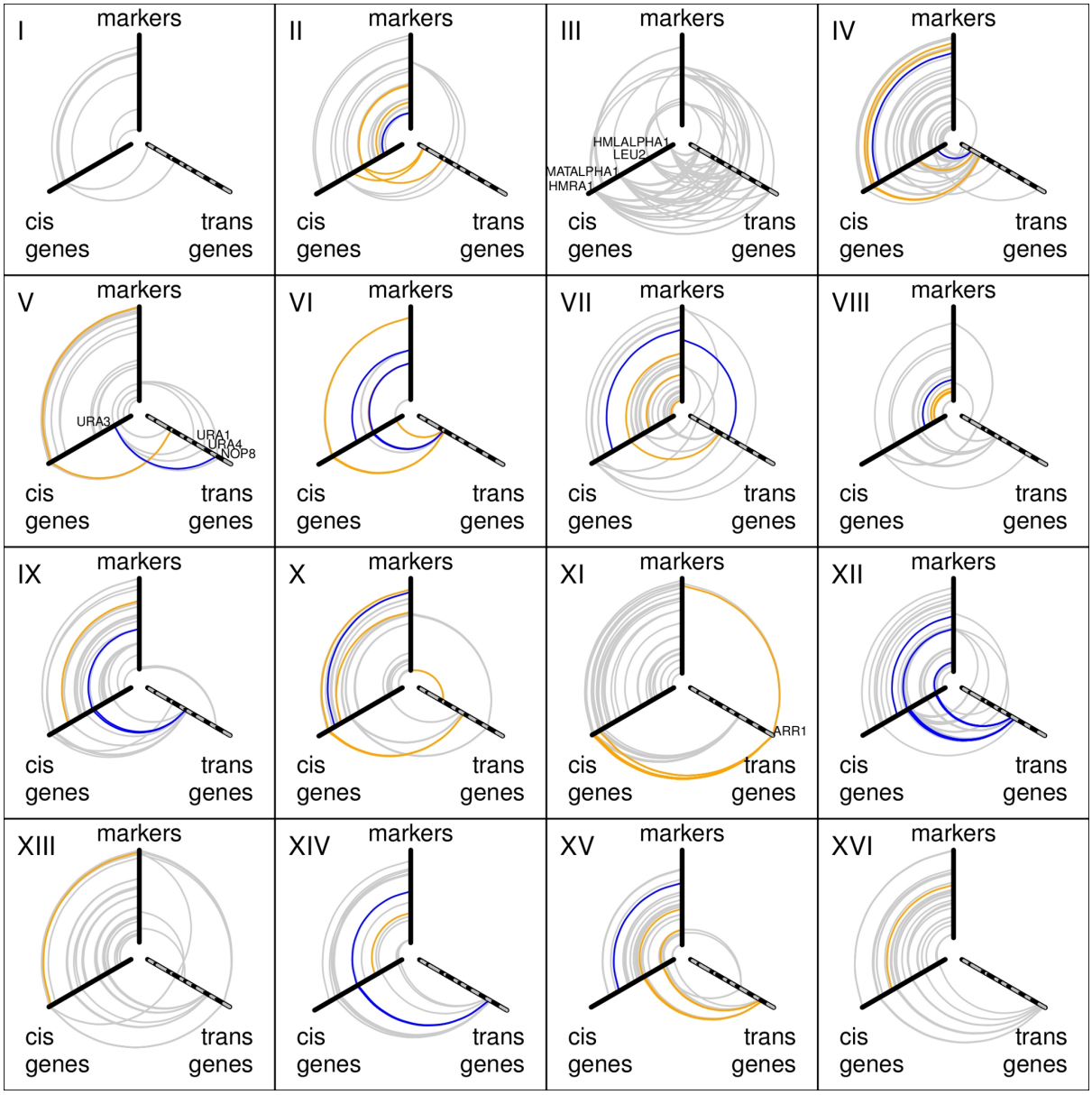

Figure 8: eQTL network of yeast. A qp-graph estimate $\hat{G}^{(\bar{q})}_{0.1}$ of the eQTL network in yeast, involving only connected components with at least one *cis* or *trans*-acting association, is shown by means of hive plots. For each chromosome, the hive plot shows three axes, where markers and genes are ordered from the center according to their genomic location. Vertical and left axes represent the chromosome in the corresponding panel, while the right axis represents the entire yeast genome alternating black and gray along consecutive chromosomes. In these plots we label the left and right axes as *cis* and *trans* to merely indicate the same chromosome or the entire genome, respectively. Edges between axes labeled as markers and *cis* genes connect eQTLs and genes located in the same chromosome, whereas edges between the markers axis and the *trans* genes axis correspond to *trans*-eQTLs affecting genes in different chromosomes. Edges between *cis* genes and *trans* genes axes correspond to gene-gene associations in $\hat{G}^{(\bar{q})}_{0.1}$. Edges whose at least one of their endpoints correspond to a transcription factor or RNA-binding coding gene, are highlighted in orange and blue, respectively. Note that lines may overlap due to an insufficient resolution of the image.

help to elucidate what fraction of them are of genetic, molecular or evolutionary origin.

Discussion

Gene expression is a high-dimensional multivariate trait whose variability is the result of genetic, molecular and environmental perturbations, and often different kinds of confounding effects. Dissecting the components of this variability and being able to adjust for some of them is a major goal to every study using genetical genomics data. Here we have used a class of statistical models with a graphical interpretation, mixed GMMs, to approach this challenge from a multivariate perspective. Using simulations we have shown that genetic effects can propagate proportionally to the marginal correlation between the genes, and that this effect may be amplified under selection bias (Fig. 1), underscoring the need to adjust for indirect associations.

Using standard linear theory and basic principles from mixed GMMs, we have derived the parameters for an exact likelihood-ratio test (LRT) on data from conditional Gaussian distributions (Fig. 2) that accommodate both linear and interaction effects between genetic variants and continuous gene expression profiles. Higher-order conditioning on mixed data unlocks a number of strategies that one may follow to disentangle direct and indirect effects in genetical genomics experiments. We exploited it by using marginal distributions and limited-order correlations, which helped to compare the genetic control of gene expression between chromosomes and throughout the gene network (Fig. 8). In particular, we could see that the degree of connections of each gene to other genes in the eQTL network correlated positively with both, the narrow-sense heritability and the fraction of variance explained by its eQTLs (Fig. 7). The larger genetic effects were in fact due to *trans*-acting eQTLs from those genes with more connections. Using those connections we were able to estimate the molecular role of two such hub genes with unknown function.

Expression data from large experimental crosses in systems genetics are becoming increasingly available to the community. This will facilitate the use of mixed GMMs for the purpose of exploring interaction effects involving genetic loci to advance our understanding of the genetic control of gene expression. The algorithms described in this article are implemented in the open source R/Bioconductor package qpgraph available for download at `http://www.bioconductor.org`. Scripts with the R code reproducing the results of this article are available at `http://functionalgenomics.upf.edu/supplements/eQTLmixedGMMs`.

Acknowledgments

This work has been supported by a grant from the Spanish Ministry of Economy and Competitiveness to R.C. (TIN2011-22826). We thank M.M. Albà, D.R. Cox, M. Francesconi, S.L. Lauritzen, B. Lehner and N. Wermuth for helpful discussions on different parts of this article. We thank R. Brem for kindly providing raw expression data files from the yeast data set analyzed in this paper.

References

[1] Michael Ashburner, Catherine A Ball, Judith A Blake, David Botstein, Heather Butler, J Michael Cherry, Allan P Davis, Kara Dolinski, Selina S Dwight, Janan T Eppig, et al. Gene ontology: tool for the unification of biology. *Nature genetics*, 25(1):25–29, 2000.

[2] Anastasia Baryshnikova, Michael Costanzo, Chad L Myers, Brenda Andrews, and Charles Boone. Genetic interaction networks: Toward an understanding of heritability. *Annual review of genomics and human genetics*, 14:111–133, 2013.

[3] Nan Bing and Ina Hoeschele. Genetical genomics analysis of a yeast segregant population for transcription network inference. *Genetics*, 170(2):533–42, Jun 2005.

[4] Joshua S Bloom, Ian M Ehrenreich, Wesley T Loo, Thúy-Lan Võ Lite, and Leonid Kruglyak. Finding the sources of missing heritability in a yeast cross. *Nature*, 494(7436):234–237, 2013.

[5] Rainer Breitling, Yang Li, Bruno M Tesson, Jingyuan Fu, Chunlei Wu, Tim Wiltshire, Alice Gerrits, Leonid V Bystrykh, Gerald de Haan, Andrew I Su, et al. Genetical genomics: spotlight on qtl hotspots. *PLoS Genetics*, 4(10):e1000232, 2008.

[6] Rachel B Brem and Leonid Kruglyak. The landscape of genetic complexity across 5,700 gene expression traits in yeast. *P Natl Acad Sci USA*, 102:1572–7, Feb 2005.

[7] Rachel B Brem, Gaël Yvert, Rebecca Clinton, and Leonid Kruglyak. Genetic dissection of transcriptional regulation in budding yeast. *Science*, 296(5568):752–755, 2002.

[8] K. W. Broman, H. Wu, S. Sen, and G. A. Churchill. R/qtl: QTL mapping in experimental crosses. *Bioinformatics*, 19:889–890, 2003.

[9] Karl W Broman and Saunak Sen. *A guide to QTL mapping with R/qtl*. Springer, 2009.

[10] Robert Castelo and Alberto Roverato. A robust procedure for Gaussian graphical model search from microarray data with p larger than n. *Journal of Machine Learning Research*, 7:2621–50, 2006.

[11] Robert Castelo and Alberto Roverato. Reverse engineering molecular regulatory networks from microarray data with qp-graphs. *Journal of Computational Biology*, 16(2):213–227, 2009.

[12] Lin S Chen, Frank Emmert-Streib, and John D Storey. Harnessing naturally randomized transcription to infer regulatory relationships among genes. *Genome Biol*, 8(10):R219, 2007.

[13] Vivian G Cheung and Richard S Spielman. Genetics of human gene expression: mapping dna variants that influence gene expression. *Nature Reviews Genetics*, 10(9):595–604, 2009.

[14] Chen-Shan Chin, Victor Chubukov, Emmitt R Jolly, Joe DeRisi, and Hao Li. Dynamics and design principles of a basic regulatory architecture controlling metabolic pathways. *PLoS Biol*, 6(6):e146, 06 2008.

[15] Hyonho Chun and Sündüz Keleş. Expression quantitative trait loci mapping with multivariate sparse partial least squares regression. *Genetics*, 182(1):79–90, 2009.

[16] Michael Costanzo, Anastasia Baryshnikova, Jeremy Bellay, Yungil Kim, Eric D Spear, Carolyn S Sevier, Huiming Ding, Judice LY Koh, Kiana Toufighi, Sara Mostafavi, et al. The genetic landscape of a cell. *science*, 327(5964):425–431, 2010.

[17] Ross E Curtis, Seyoung Kim, John L Woolford Jr, Wenjie Xu, and Eric P Xing. Structured association analysis leads to insight into Saccharomyces cerevisiae gene regulation by finding multiple contributing eqtl hotspots associated with functional gene modules. *BMC Genomics*, 14(196):1–17, 2013.

[18] Vanessa Didelez and David Edwards. Collapsibility of graphical cg-regression models. *Scandinavian Journal of Statistics*, 31(4):535–551, 2004.

[19] D. Edwards. *Introduction to graphical modelling.* Springer, 2000.

[20] David Edwards, Gabriel C G de Abreu, and Rodrigo Labouriau. Selecting high-dimensional mixed graphical models using minimal aic or bic forests. *BMC Bioinformatics*, 11:18, 2010.

[21] Benjamin P Fairfax, Seiko Makino, Jayachandran Radhakrishnan, Katharine Plant, Stephen Leslie, Alexander Dilthey, Peter Ellis, Cordelia Langford, Fredrik O Vannberg, and Julian C Knight. Genetics of gene expression in primary immune cells identifies cell type-specific master regulators and roles of hla alleles. *Nature genetics*, 44(5):502–510, 2012.

[22] R. Grone, CR Johnson, EM Sá, and H. Wolkowicz. Positive definite completions of partial Hermitian matrices. *Linear Algebra Applic.*, 58:109–124, 1984.

[23] Frank Grosveld, Greet Blom van Assendelft, David R Greaves, and George Kollias. Position-independent, high-level expression of the human β-globin gene in transgenic mice. *Cell*, 51(6):975–985, 1987.

[24] F. Harary. *Graph theory*. Addison-Wesley, 1969.

[25] Trevor Hastie, Robert Tibshirani, and Jerome Friedman. *The elements of statistical learning*. Springer, 2009.

[26] Ritsert C Jansen and Jan-Peter Nap. Genetical genomics: the added value from segregation. *TRENDS in Genetics*, 17(7):388–390, 2001.

[27] Markus Kalisch and Peter Bühlmann. Estimating high-dimensional directed acyclic graphs with the pc-algorithm. *The Journal of Machine Learning Research*, 8:613–636, 2007.

[28] Eun Yong Kang, Chun Ye, Ilya Shpitser, and Eleazar Eskin. Detecting the presence and absence of causal relationships between expression of yeast genes with very few samples. *J Comput Biol*, 17(3):533–46, Mar 2010.

[29] Hyun Min Kang, Chun Ye, and Eleazar Eskin. Accurate discovery of expression quantitative trait loci under confounding from spurious and genuine regulatory hotspots. *Genetics*, 180(4):1909–25, Dec 2008.

[30] CM Kendziorski, M Chen, M Yuan, H Lan, and AD Attie. Statistical methods for expression quantitative trait loci (eqtl) mapping. *Biometrics*, 62(1):19–27, 2006.

[31] Seyoung Kim and Eric P Xing. Statistical estimation of correlated genome associations to a quantitative trait network. *PLoS Genet*, 5(8):e1000587, Aug 2009.

[32] Martin Krzywinski, Inanc Birol, Steven JM Jones, and Marco A Marra. Hive plotsrational approach to visualizing networks. *Briefings in Bioinformatics*, 13(5):627–644, 2012.

[33] S.L. Lauritzen. *Graphical Models*. Oxford University Press, 1996.

[34] S.L. Lauritzen and N. Wermuth. Graphical models for associations between variables, some of which are qualitative and some quantitative. *Annals of Statistics*, 17(1):31–57, 1989.

[35] Sang Hong Lee, Naomi R Wray, Michael E Goddard, and Peter M Visscher. Estimating missing heritability for disease from genome-wide association studies. *The American Journal of Human Genetics*, 88(3):294–305, 2011.

[36] Jeffrey T Leek, Robert B Scharpf, Héctor Corrada Bravo, David Simcha, Benjamin Langmead, W Evan Johnson, Donald Geman, Keith Baggerly, and Rafael A Irizarry. Tackling the widespread and critical impact of batch effects in high-throughput data. *Nature Reviews Genetics*, 11(10):733–739, 2010.

[37] Jeffrey T Leek and John D Storey. Capturing heterogeneity in gene expression studies by surrogate variable analysis. *PLoS Genetics*, 3(9):e161, 2007.

[38] EL Lehman and JP Romano. *Testing statistical hypotheses*. Springer-Verlag, 2005.

[39] Qiliang Li, Kenneth R Peterson, Xiangdong Fang, and George Stamatoyannopoulos. Locus control regions. *Blood*, 100(9):3077–3086, 2002.

[40] Jennifer Listgarten, Carl Kadie, and David Heckerman. Correction for hidden confounders in the genetic analysis of gene expression. *Proceedings of the National Academy of Sciences*, 107(38):16465–16470, September 2010.

[41] Bing Liu, Alberto de la Fuente, and Ina Hoeschele. Gene network inference via structural equation modeling in genetical genomics experiments. *Genetics*, 178(3):1763–76, Mar 2008.

[42] Jacob J Michaelson, Rudi Alberts, Klaus Schughart, and Andreas Beyer. Data-driven assessment of eqtl mapping methods. *BMC genomics*, 11(1):502, 2010.

[43] Stephen B Montgomery, Micha Sammeth, Maria Gutierrez-Arcelus, Radoslaw P Lach, Catherine Ingle, James Nisbett, Roderic Guigo, and Emmanouil T Dermitzakis. Transcriptome genetics using second generation sequencing in a caucasian population. *Nature*, 464(7289):773–777, 2010.

[44] Elias Chaibub Neto, Christine T Ferrara, Alan D Attie, and Brian S Yandell. Inferring causal phenotype networks from segregating populations. *Genetics*, 179(2):1089–100, Jun 2008.

[45] Elias Chaibub Neto, Mark P Keller, Alan D Attie, and Brian S Yandell. Causal graphical models in systems genetics: a unified framework for joint inference of causal network and genetic architecture for correlated phenotypes. *Ann Appl Stat*, 4(1):320–339, Mar 2010.

[46] PS Nielsen, B van den Hazel, T Didion, M de Boer, M Jrgensen, RJ Planta, MC Kielland-Brandt, and HA Andersen. Transcriptional regulation of the saccharomyces cerevisiae amino acid permease gene bap2. *Molecular & general genetics*, 264(5):613–622, 2001.

[47] Leopold Parts, Oliver Stegle, John Winn, and Richard Durbin. Joint genetic analysis of gene expression data with inferred cellular phenotypes. *PLoS Genet*, 7(1):e1001276, 2011.

[48] Enrico Petretto, Jonathan Mangion, Nicholas J Dickens, Stuart A Cook, Mande K Kumaran, Han Lu, Judith Fischer, Henrike Maatz, Vladimir Kren, Michal Pravenec, et al. Heritability and tissue specificity of expression quantitative trait loci. *PLoS genetics*, 2(10):e172, 2006.

[49] C.R. Rao. *Linear Statistical Inference and Its Applications*. John Wiley & Sons, 1973.

[50] Matthew V Rockman. Reverse engineering the genotype–phenotype map with natural genetic variation. *Nature*, 456(7223):738–744, 2008.

[51] Matthew V Rockman and Leonid Kruglyak. Genetics of global gene expression. *Nature Reviews Genetics*, 7(11):862–872, 2006.

[52] A. Roverato. Hyper inverse Wishart distribution for non-decomposable graphs and its application to Bayesian inference for Gaussian graphical models. *Scandinavian Journal of Statistics*, 29(3):391–411, 2002.

[53] Eric E Schadt, Stephanie A Monks, Thomas A Drake, Aldons J Lusis, Nam Che, Veronica Colinayo, Thomas G Ruff, Stephen B Milligan, John R Lamb, Guy Cavet, et al. Genetics of gene expression surveyed in maize, mouse and man. *Nature*, 422(6929):297–302, 2003.

[54] G.A.F. Seber. *A matrix handbook for statisticians*. Wiley-Interscience, 2007.

[55] G. Smyth. limma: Linear models for microarray data. In *Bioinformatics and Computational Biology Solutions Using R and Bioconductor*, Statistics for Biology and Health, pages 397–420. Springer New York, 2005.

[56] A Steger and N.C. Wormald. Generating random regular graphs quickly. *Comb Probab Comput*, 8(4):377–96, 1999.

[57] Oliver Stegle, Leopold Parts, Richard Durbin, and John Winn. A bayesian framework to account for complex non-genetic factors in gene expression levels greatly increases power in eqtl studies. *PLoS computational biology*, 6(5):e1000770, 2010.

[58] Bruno M Tesson and Ritsert C Jansen. eQTL analysis in mice and rats. In *Cardiovascular Genomics*, volume 573 of *Methods in Molecular Biology*, pages 285–309. Springer, 2009.

[59] Harm-Jan Westra, Marjolein J Peters, Tõnu Esko, Hanieh Yaghootkar, Claudia Schurmann, Johannes Kettunen, Mark W Christiansen, Benjamin P Fairfax, Katharina Schramm, Joseph E Powell, et al. Systematic identification of trans eQTLs as putative drivers of known disease associations. *Nature genetics*, 45(10):1238–1243, 2013.

[60] Gael Yvert, Rachel B Brem, Jacqueline Whittle, Joshua M Akey, Eric Foss, Erin N Smith, Rachel Mackelprang, and Leonid Kruglyak. Trans-acting regulatory variation in saccharomyces cerevisiae and the role of transcription factors. *Nature Genetics*, 35:57–64, 2003.

[61] J Zhu, P Y Lum, J Lamb, D GuhaThakurta, S W Edwards, R Thieringer, J P Berger, M S Wu, J Thompson, A B Sachs, and E E Schadt. An integrative genomics approach to the reconstruction of gene networks in segregating populations. *Cytogenet Genome Res*, 105(2-4):363–74, 2004.

Supplementary material

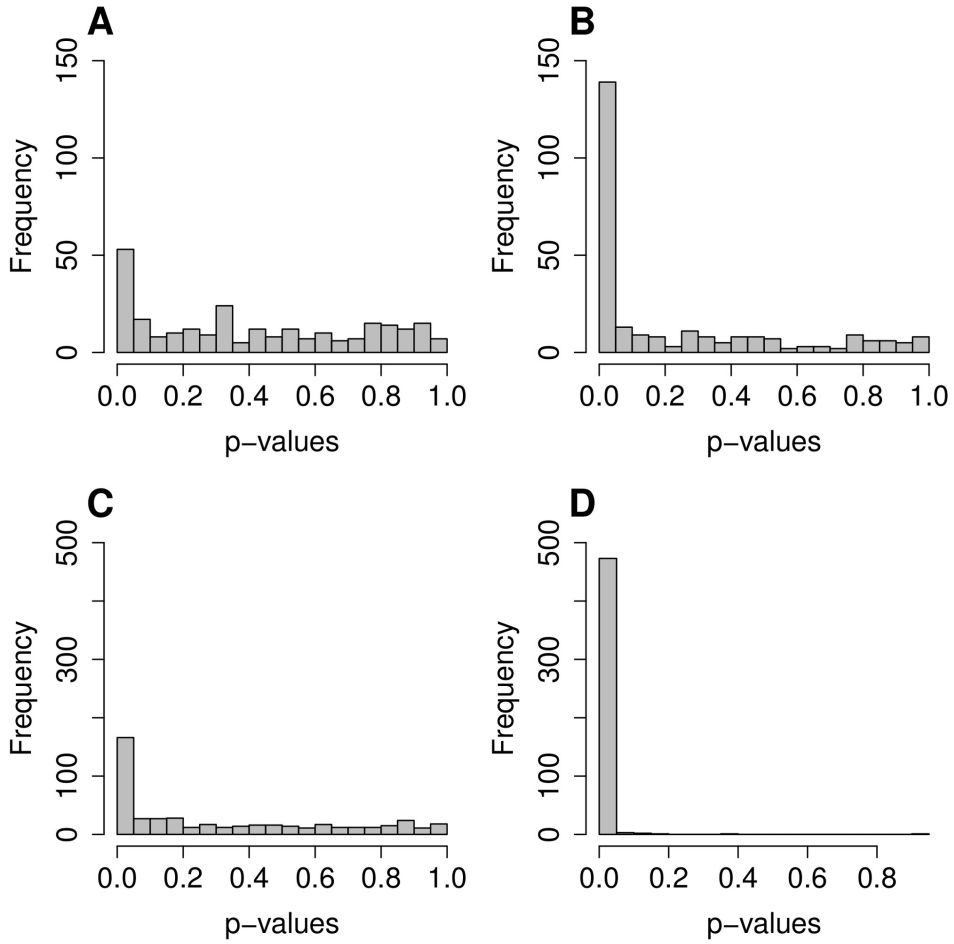

Figure S1: Fit of gene models with *trans*-eQTLs to yeast data. Distribution of p-values for the F-test between sparser qp-graph $\hat{G}^{(\bar{q})}_{0.1}$ (null) models and larger single marker (alternative) models. Null qp-graph models were derived from genes γ with *trans*-eQTLs δ located at a minimum distance of 10kb from the target gene, and found significant by single marker regression at a genome-wide $p < 0.01$ and discarding those with NRR $\hat{\nu}^{\bar{q}}_{\gamma\delta} > 0.1$. Panel (A) contains p-values from 269 genes with at least one *trans*-eQTL in $\hat{G}^{(\bar{q})}_{0.1}$. Panel (B) results from using the same alternative $\hat{G}^{(0)}$ models as in (A) but replacing eQTLs δ in null models by different ones δ' randomly selected among those in the alternative models. Panel (C) contains p-values from 481 genes γ with no *trans*-eQTL in $\hat{G}^{(\bar{q})}_{0.1}$ but connected to at least one other gene in $\hat{G}^{(\bar{q})}_{0.1}$. In this case, genes η in $\hat{G}^{(\bar{q})}_{0.1}$ whose $\hat{\nu}^{\bar{q}}_{\gamma\eta} < 0.1$ where included in both, the null and the alternative models. Panel (D) results from using the same alternative $\hat{G}^{(0)}$ models as in (C) but replacing genes η in null models by different ones η' randomly selected among the rest of the genes in the data set. The vast majority of tests in (A, C) have $p > 0.05$, thus indicating that denser alternative gene models derived from single marker regression $\hat{G}^{(0)}$ do not fit the data significantly better than the sparser null models derived from qp-graph estimates $\hat{G}^{(\bar{q})}_{0.1}$. This fact changes substantially in the control experiments shown in (B, D).

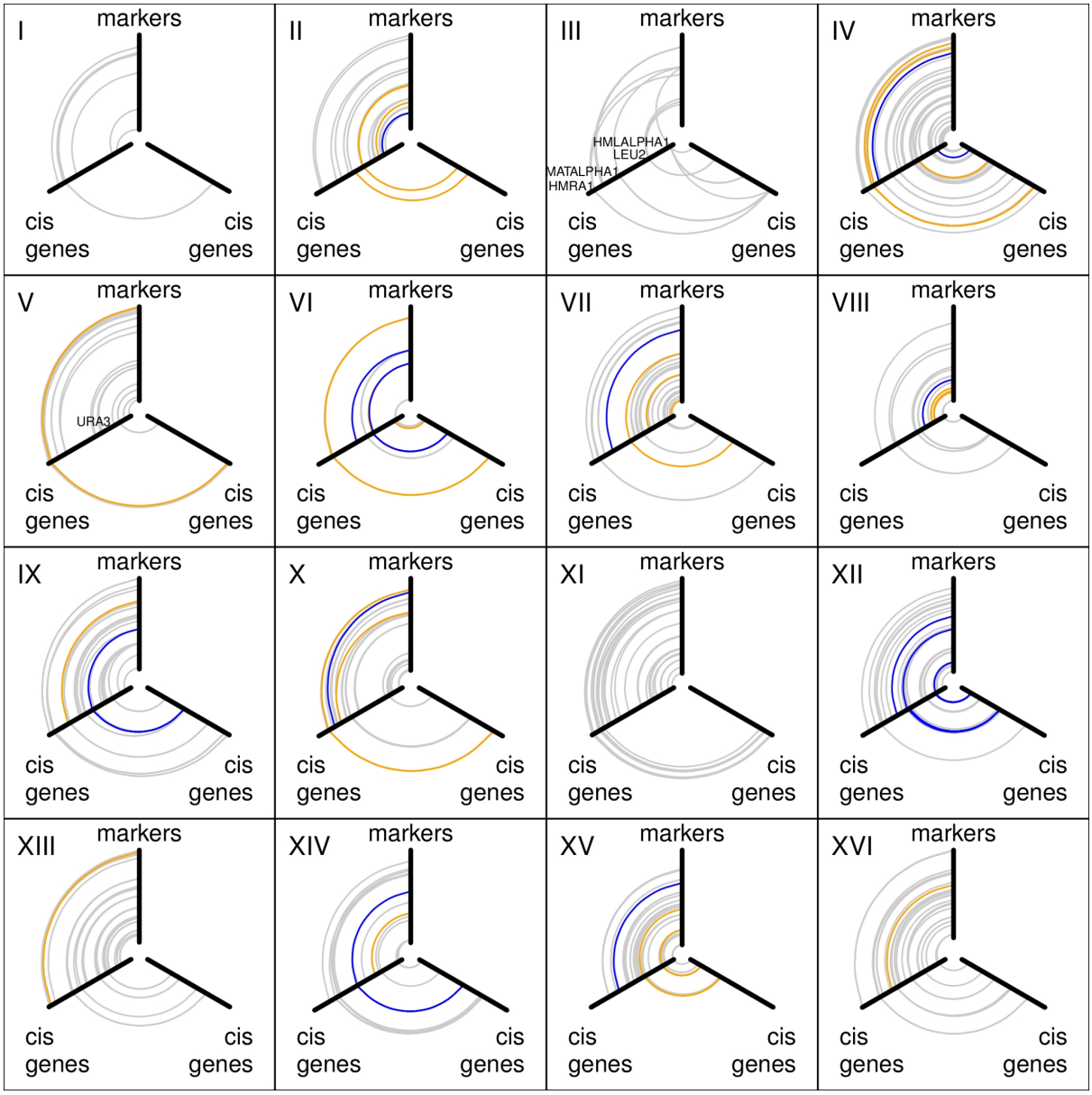

Figure S2: eQTL network of yeast. A qp-graph estimate $\hat{G}^{(\bar{q})}_{0.1}$ of the eQTL network in yeast, involving only connected components with at least one *cis* or *trans*-acting association, is shown by means of hive plots. For each chromosome, the hive plot shows three axes, where markers and genes are ordered from the center according to their genomic location. All axes represent the chromosome in the corresponding panel. In these plots we label the left and right axes as *cis* to merely indicate the same chromosome. Edges between the axis labeled as markers and the left *cis*-genes axis connect eQTLs and genes located in the same chromosome. Edges between the two *cis* genes axes correspond to gene-gene associations in $\hat{G}^{(\bar{q})}_{0.1}$ between genes from the same chromosome. Edges whose at least one of their endpoints correspond to a transcription factor or RNA-binding coding gene, are highlighted in orange and blue, respectively. Note that lines may overlap due to an insufficient resolution of the image.

Table S1: Gene Ontology (GO) enrichment of genes in the eQTLnetwork connected to the gene of unknown function *YLR040C*. GO terms below are reported on the basis of a conditional hypergeometric test, applying Holm's correction to raw p-values, selecting those with corrected $p < 0.01$ and discarding GO terms with less than 3 genes in either the term (col. "Size") or overlapping with the genes connected to *YLR040C* (col. "Cnt").

Term	OR	ExpCnt	Cnt	Size	Padj	Genes
pheromone-dependent signal transduction involved in conjugation with cellular fusion	76.8	0.1	3	30	4.5E-04	MF(ALPHA)1, STE2, STE3
sex determination	64.7	0.1	3	35	6.9E-04	HMLALPHA1, HMLALPHA2, MATALPHA1
cell fate commitment	64.7	0.1	3	35	6.9E-04	HMLALPHA1, HMLALPHA2, MATALPHA1
cellular response to pheromone	60.9	0.2	5	80	5.8E-06	BAR1, MF(ALPHA)1, SAG1, STE2, STE3
cell surface receptor signaling pathway	54.4	0.1	3	41	9.4E-04	MF(ALPHA)1, STE2, STE3
response to organic substance	37.6	0.4	6	178	9.5E-06	BAR1, MF(ALPHA)1, SAG1, STE2, STE3, STE6
multi-organism cellular process	35.1	0.3	5	134	6.8E-05	BAR1, MF(ALPHA)1, SAG1, STE2, STE3
cellular process involved in reproduction	30.5	0.7	7	402	2.2E-05	BAR1, HMLALPHA1, HMLALPHA2, MATALPHA1, MF(ALPHA)1, STE2, STE3
conjugation with cellular fusion	29.7	0.2	3	95	4.5E-03	BAR1, MF(ALPHA)1, SAG1
biological regulation	23.7	3.3	10	1657	7.3E-04	BAR1, BST1, GYP8, HMLALPHA1, HMLALPHA2, MATALPHA1, MF(ALPHA)1, STE2, STE3, STE6
reproductive process	19.5	0.3	4	162	2.5E-03	HMLALPHA1, HMLALPHA2, MATALPHA1, MF(ALPHA)1
cellular response to chemical stimulus	15.9	0.6	5	281	1.7E-03	BAR1, MF(ALPHA)1, SAG1, STE2, STE3

Table S2: Gene Ontology (GO) enrichment (biological process) on the genes in the eQTLnetwork connected to the gene of unknown function *YCR097W-A*. GO terms below are reported on the basis of a conditional hypergeometric test, applying Holm's correction to raw p-values, selecting those with corrected $p < 0.01$ and discarding GO terms with less than 3 genes in either the term (column "Size") or overlapping with the genes connected to *YCR097W-A* (column "Cnt").

Term	**OR**	**ExpCnt**	**Cnt**	**Size**	**Padj**	**Genes**
pheromone-dependent signal transduction involved in conjugation with cellular fusion	106.3	0.1	4	30	6.9E-06	MFA2, MF(ALPHA)1, STE2, STE3
cell surface receptor signaling pathway	74.6	0.1	4	41	2.4E-05	MFA2, MF(ALPHA)1, STE2, STE3
cellular response to pheromone	74.1	0.2	6	80	1.5E-07	AGA2, BAR1, MFA2, MF(ALPHA)1, STE2, STE3
response to organic substance	44.1	0.4	7	178	4.8E-07	AGA2, BAR1, MFA2, MF(ALPHA)1, STE2, STE3, STE6
multi-organism cellular process	42.4	0.3	6	134	3.1E-06	AGA2, BAR1, MFA2, MF(ALPHA)1, STE2, STE3
conjugation with cellular fusion	40.0	0.2	4	95	2.6E-04	AGA2, BAR1, MFA2, MF(ALPHA)1
cellular process involved in reproduction	22.8	0.8	7	402	4.8E-05	BAR1, HMRA1, MATALPHA1, MFA2, MF(ALPHA)1, STE2, STE3
cellular response to chemical stimulus	19.2	0.6	6	281	2.0E-04	AGA2, BAR1, MFA2, MF(ALPHA)1, STE2, STE3
single organism signaling	14.0	0.6	5	274	2.5E-03	BAR1, MFA2, MF(ALPHA)1, STE2, STE3
biological regulation	11.9	3.6	10	1657	2.6E-03	BAR1, BST1, GYP8, HMRA1, MATALPHA1, MFA2, MF(ALPHA)1, STE2, STE3, STE6
response to stimulus	8.1	2.4	8	1107	7.1E-03	AGA2, BAR1, MFA2, MF(ALPHA)1, STE2, STE3, STE6